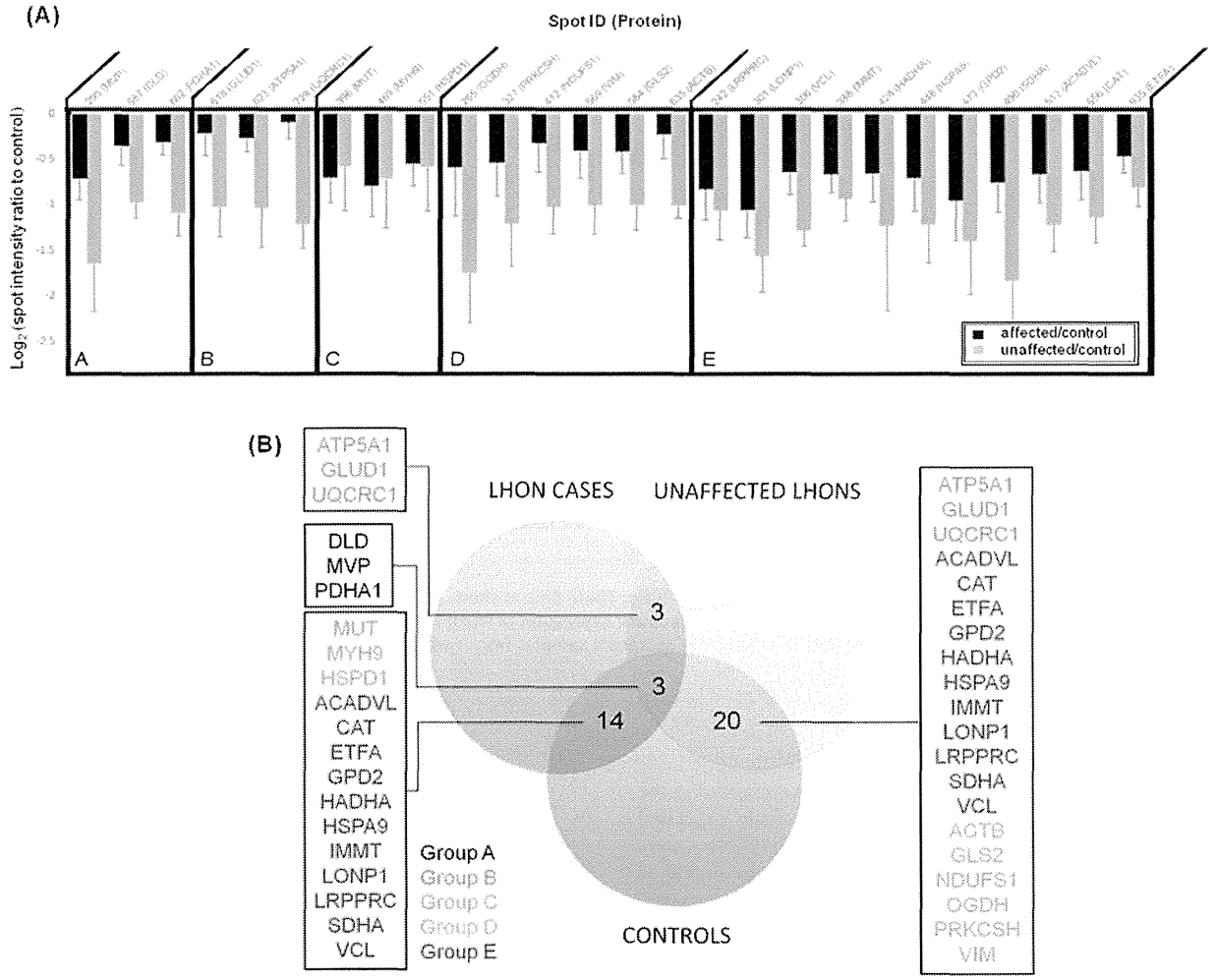

Figure 7. (A) A plot of log-ratio spot intensities, comparing affected individuals (black bars) and unaffected relatives (grey bars) versus controls. Log-ratios of protein spot intensities were plotted according to the method of [63]. In the case that one protein was identified in several spots, the only spot intensity that gave the highest significant value was selected for this plot. Negative changes were observed in all discoveries. Group A includes protein spots which were significantly differentially expressed in comparisons of affected and unaffected carriers, affected individuals and controls, and unaffected individuals and controls (Post Hoc Tukey Test; *P*-value<0.05). Group B includes protein spots which were significantly differentially expressed in comparisons of affected and unaffected carriers, and between unaffected carriers and controls. Changes between affected individuals and controls were not significant. Group C includes protein spots which were significantly differentially expressed only in the comparison between affected individuals and control. Group D includes protein spots which were significantly differentially expressed only in the comparison between unaffected carriers and controls. Group E includes protein spots which were significantly differentially expressed the comparisons between affected individuals and controls, and between unaffected carriers and controls. Here, the differences in expression between affected and unaffected carriers are not significantly different. **(B) Venn diagram representation of proteins identified in three comparisons derived from figure 7A.**
doi:10.1371/journal.pone.0106779.g007

Given the decreased levels of metabolic and OXPHOS related proteins in mutation carriers in the present study, it is likely that aerobic respiration is particularly affected in LHON mutant fibroblasts. To further support this notion, ETFA electron transfer flavoprotein subunit alpha was down regulated in the fibroblasts of both affected and unaffected mutation carriers. This protein is important in transferring electrons from many of the mitochondrial flavoprotein dehydrogenases to the respiratory chain [41]. This bioenergetic dysfunction is consistent with previous reports of defective energy metabolism in LHON mutant fibroblasts, including reduction of complex I activity, poor respiratory capacity and reduced ATP content in mutants compared to controls [42,43].

Several stability and transport proteins were also differentially expressed: heat shock protein 60 (HSPD1), Stress-70 protein (MTHSP75/HSPA9) and lon protease 1 (LONP1) (Table 2 and 3). HSPD1 is one of the most important chaperonins inside the mitochondrial matrix. It facilitates correct folding and prevents mis-folding of unfolded proteins formed under mitochondrial stress [44]. Mutations of HSPD1 in hereditary spastic paraplegia and MitChap60 disease highlight possible implications for neurodegenerative disease [45–47]. In the present study, expression of HSPD1 was reduced 1.5 fold in LHON case fibroblasts compared to unrelated controls. This reduction may have deleterious consequences if it happens in neuronal retinal ganglion cells, since they are post-mitotic and are highly susceptible to the

Table 6. Differentially expressed proteins which show similar trends of down-regulation in the mitochondrial proteomes of both LHON cases and unaffected relatives when compared with controls.

Name of Protein	Cellular pathway or function involved
Glycerol-3-phosphate dehydrogenase	Intermediary metabolism: transferring reducing equivalents to mitochondrial repiratory chain
Dihydrolipoyl dehydrogenase	Intermediary metabolism: TCA cycle; generation of reducing equivalents for OXPHOS
Pyruvate dehydrogenase E1 component subunit alpha	Intermediary metabolism: carbohydrate; generation of reducing equivalents for OXPHOS
Trifunctional enzyme subunit alpha	Intermediary metabolism: lipid; β-oxidation; generation of reducing equivalents for OXPHOS
Very long-chain specific acyl-CoA dehydrogenase	Intermediary metabolism: lipid; β-oxidation; generation of reducing equivalents for OXPHOS
Succinate dehydrogenase [ubiquinone] flavoprotein subunit	Intermediary metabolism: TCA cycle; generation of reducing equivalents for OXPHOS
Electron transfer flavoprotein subunit alpha	Transfer electron from flavoprotein to OXPHOS
Mitofilin	Cristae remodeling
Lon protease 1	Protein stability and degradation
Stress-70 protein/Heat shock 70 kDa protein 9/MTHSP75	Protein stability and degradation
Catalase	Anti-oxidant enzyme
Leucine-rich PPR motif-containing protein	Mitochondrial gene expression
Vinculin	Cytoskelon
Major vault protein	Signal transduction

doi:10.1371/journal.pone.0106779.t006

accumulation of unfolded proteins [48]. Another chaperone Stress-70 protein (MTHSP75/HSPA9) was down-regulated in fibroblasts of both affected and unaffected mutation carriers compared with controls. In addition, HSPA1, HSPA9 and LONP1 co-occurred as differentially expressed proteins in other cellular models [49]. They are the components of the mitochondrial protein quality control system which protects the formation of the unfolded protein with chaperones and clears protein aggregates with proteases [50]. There can be detrimental consequences when the system is under-expressed, as found in the 11778G>A fibroblasts of the present study.

In addition to the proteomic changes in metabolic enzymes and the protein quality control system, some proteins controlling mitochondrial gene expression were also down-regulated in the mutation carriers: Leucine-rich pentatricopeptide repeat motif-containing protein (LRPPRC) and LONP1. LRPPRC was down-regulated in the fibroblasts of both affected and unaffected carriers of 11778G>A. It is a disease modifier in Leigh syndrome French-Canadian type [51]. Silencing of *LRPPRC* was associated with reduction of mitochondrial proteins including mitochondrial and nuclear encoded subunits of OXPHOS [52]. LONP1, a nucleoid protein, was also under-expressed in mutant cells. LONP1 binds to mtDNA, and its level influences a cell's sensitivity to mtDNA damage [53], with potential implications for LHON pathogenesis.

Apart from proteins involved in bioenergetic pathways and mitochondrial protein quality control, catalase and mitofilin were also differentially expressed. Compared to controls, catalase was down-regulated in both affected and unaffected fibroblasts carrying 11778G>A. Though it is mainly located in the peroxisome [54], it is also associated with mitochondria in some cell types [55,56]. Reduction or absence of catalase under oxidative stress in mitochondria can lead to the inefficient degradation of H_2O_2, leading to potential mitochondrial and cellular damage [57].

Mitofilin, a protein which plays a role in/influences cristae morphology and nucleoid structure, was down-regulated. Previously, down-regulation of mitofilin was observed in dopamine induced oxidative stress [58] and MPTP induced complex I inhibition [59]. Since oxidative stress and complex I inhibition are associated with LHON mutations, the down-regulation of mitofilin in 11778G>A mutant cells may have a role in LHON pathogenesis.

It is interesting to observe the similarities in fibroblast mitochondrial protein expression profiles between affected and unaffected 11778G>A carriers, in comparison with the unrelated controls. The levels of 14 (out of total 27) identified proteins were reduced both in the affected and the unaffected mutation carriers compared to the controls (Table 6). The proteins down-regulated in both groups of 11778 mutant fibroblasts were electron transfer flavoprotein, succinate dehydrogenase, dihydrolipoyl dehydrogenase, subunit of pyruvate dehydrogenase, glycerol-3-phosphate dehydrogenase concerned with electron transfer and aerobic respiration, very long chain specific acyl-CoA dehydrogenase, trifunctional plasma enzyme of β-oxidation, chaperonins such as lon protease 1, heat-shock protein-70, leucine-rich PPR motif-containing protein, mitofilin, catalase and some other proteins (Table 6). This similarity might reflect common compensatory responses cells responding similarly to the same adverse conditions, regardless of whether the cells come from affected or unaffected individuals. Since 11778G>A mutant fibroblasts have been shown to have reduced complex I activity and larger bioenergetic defects [43], these reduced levels of protein expression might be due to degradation of proteins with poor performance or to alteration of nuclear gene responses in the

presence of OXPHOS deficiency. These mechanisms would be consistent with the observed results: that the cells in primary fibroblasts cultures encountering the 11778G>A mutation respond similarly to the adverse consequences of the mutation, regardless of the phenotypic status of the person who provided the biopsy. This mutation might reprogram gene expression profiles, with similar consequent physiological states of the cells driving similar proteome changes between the carriers. Similar transcriptomic profiles have been observed in previous studies, where clinically affected and unaffected tissues from the same individual have similar profiles [60].

There are some previous studies on transcriptomal changes in LHON mutant cells using various cell types. However, they reported differing patterns of transcriptomal changes, possibly reflecting differences in susceptibility to bioenergetic derangements between cell types. For instance, transcriptomic changes from osteosarcoma-derived LHON cybrids and LHON-mutant lymphoblastoid cell lines generally showed different profiles, with the exception of nine common genes [17,19]. Differentially expressed gene products involved in transcription and transport processes were reported in the lymphocytes of four Saudi Arab LHON patients [18]. None of these gene products was differentially expressed in our data. This could be due the employment of different cell types (fibroblasts versus osteosarcoma derived cybrids or lymphoblastoid cell lines), different sub-cellular locations that we are observing (enrichment of mitochondrial proteins in our study versus global expression profiling), or different patterns of expression at the RNA level and the protein level, because of post-translational modifications, degradation and dependence on organellar transport. Consequently, we did not find any evidence of ER stress or protein unfolding responses, which are observed in various mitochondrial diseases [19].

This study which, to the best of our knowledge, is the first study to profile mitochondrial proteomes in LHON, has some limitations. One potential limitation is the challenge of selecting well age-and sex-matched controls for cases and their related unaffected individuals. We selected pedigrees in which the unaffected individuals were well above the age of onset of their affected relatives for each particular family (Table 1). All of the three unaffected relatives, U1 from pedigree F1 (30 years old at present), U2 from pedigree F9 (21 years old at present) and U3 (49 years old at present) from pedigree F66 were above both the mean age of onset for Thai individuals (20.7±10.0 years for males and 28.6±14.6 years for females) [61], and the mean age of onset within their families, 13 years, 17 years and 32 years respectively. None of them have developed the disease, and their latest eye examinations in early 2014 were within normal limits. Another potential limitation was that not all of the unaffected individuals were of the same sex: two were male and one was female. Sex differences could potentially confound the results, especially in the comparisons between unaffected mutation carriers and controls. Nevertheless, in spite of these limitations, the results from the present study could contribute to extant understanding of proteome changes in LHON mutant cells.

In summary, our proteomic data highlight proteins that were differentially expressed between the fibroblast of LHON cases, unaffected carriers of the LHON 11778G>A primary mtDNA mutation, and normal individuals. Functional analyses of these proteins imply that bioenergetic derangements and poor protein quality control systems, both incompatible with regular functioning of retinal ganglion cells, may be involved in LHON pathogenesis. Failure to conduct proper protein folding, to assemble protein complexes properly and to prevent unfolded proteins having damaging effects on cells may lead to the onset of LHON.

Supporting Information

Figure S1 The three pedigrees used in the present study. (A = LHON cases and U = unaffected relatives whose fibroblasts were used in the present study. The arrow indicates the proband of each pedigree).
(DOCX)

Acknowledgments

We would like to express our gratitude to Dr. Nopasak Phasukkijwatana, Dr. Lanka Ranaweera, Dr. Hathaichanoke Boonyarit, Dr. Somchai Chutipongtanate, Dr. Kitisak Sintiprungrat, Ms. Bussaraporn Kunhapan, Ms. Rochmy Istikharah, Mr. Yutthana Joyjinda for their technical assistance and to Dr. James Stankovich for the proofreading of the manuscript and to Jatuphon Nakhonsri for the illustration of figure 7. We sincerely thank all the LHON patients, their family members and all individuals in the control group for sample collection.

Author Contributions

Conceived and designed the experiments: AWT VT PL. Performed the experiments: AWT SC SK WK MK TT. Analyzed the data: AWT CP VT PL. Contributed reagents/materials/analysis tools: VT. Wrote the paper: AWT VT PL. Clinical evaluation: WC. Initiated the research project: PL. Collected samples: PL.

References

1. Man PY, Griffiths PG, Brown DT, Howell N, Turnbull DM, et al. (2003) The epidemiology of Leber hereditary optic neuropathy in the North East of England. Am J Hum Genet 72: 333–339.
2. Harding AE, Sweeney MG, Govan GG, Riordan-Eva P (1995) Pedigree analysis in Leber hereditary optic neuropathy families with a pathogenic mtDNA mutation. Am J Hum Genet 57: 77–86.
3. Carelli V, La Morgia C, Iommarini L, Carroccia R, Mattiazzi M, et al. (2007) Mitochondrial optic neuropathies: how two genomes may kill the same cell type? Biosci Rep 27: 173–184.
4. Yen MY, Wang AG, Wei YH (2006) Leber's hereditary optic neuropathy: a multifactorial disease. Prog Retin Eye Res 25: 381–396.
5. Chuenkongkaew WL, Lertrit P, Poonyathalang A, Sura T, Ruangvaravate N, et al. (2001) Leber's hereditary optic neuropathy in Thailand. Jpn J Ophthalmol 45: 665–668.
6. Chuenkongkaew W, Lertrit P, Suphavilai R (2004) Case report: A Thai patient with Leber's hereditary optic neuropathy linked to mitochondrial DNA 14484 mutation. Southeast Asian J Trop Med Public Health 35: 167–168.
7. Harding AE, Riordan-Eva P, Govan GG (1995) Mitochondrial DNA diseases: genotype and phenotype in Leber's hereditary optic neuropathy. Muscle Nerve 3: S82–84.
8. Kirkman MA, Yu-Wai-Man P, Korsten A, Leonhardt M, Dimitriadis K, et al. (2009) Gene-environment interactions in Leber hereditary optic neuropathy. Brain 132: 2317–2326.
9. Istikharah R, Tun AW, Kaewsutthi S, Aryal P, Kunhapan B, et al. (2013) Identification of the variants in PARL, the nuclear modifier gene, responsible for the expression of LHON patients in Thailand. Exp Eye Res 116C: 55–57.
10. Shankar SP, Fingert JH, Carelli V, Valentino ML, King TM, et al. (2008) Evidence for a novel x-linked modifier locus for leber hereditary optic neuropathy. Ophthalmic Genet 29: 17–24.
11. Ji Y, Zhang AM, Jia X, Zhang YP, Xiao X, et al. (2008) Mitochondrial DNA haplogroups M7b1'2 and M8a affect clinical expression of leber hereditary optic neuropathy in Chinese families with the m.11778G->a mutation. Am J Hum Genet 83: 760–768.
12. Hudson G, Keers S, Yu Wai Man P, Griffiths P, Huoponen K, et al. (2005) Identification of an X-chromosomal locus and haplotype modulating the phenotype of a mitochondrial DNA disorder. Am J Hum Genet 77: 1086–1091.
13. Kaewsutthi S, Phasukkijwatana N, Joyjinda Y, Chuenkongkaew W, Kunhapan B, et al. (2011) Mitochondrial Haplogroup Background May Influence Southeast Asian G11778A Leber Hereditary Optic Neuropathy. Invest Ophthalmol Vis Sci.

14. Hudson G, Yu-Wai-Man P, Zeviani M, Chinnery PF (2009) Genetic variation in the methylenetetrahydrofolate reductase gene, MTHFR, does not alter the risk of visual failure in Leber's hereditary optic neuropathy. Mol Vis 15: 870–875.
15. Petruzzella V, Tessa A, Torraco A, Fattori F, Dotti MT, et al. (2007) The NDUFB11 gene is not a modifier in Leber hereditary optic neuropathy. Biochem Biophys Res Commun 355: 181–187.
16. Beretta S, Mattavelli L, Sala G, Tremolizzo L, Schapira AH, et al. (2004) Leber hereditary optic neuropathy mtDNA mutations disrupt glutamate transport in cybrid cell lines. Brain 127: 2183–2192.
17. Danielson SR, Carelli V, Tan G, Martinuzzi A, Schapira AH, et al. (2005) Isolation of transcriptomal changes attributable to LHON mutations and the cybridization process. Brain 128: 1026–1037.
18. Abu-Amero KK, Jaber M, Hellani A, Bosley TM (2010) Genome-wide expression profile of LHON patients with the 11778 mutation. Br J Ophthalmol 94: 256–259.
19. Cortopassi G, Danielson S, Alemi M, Zhan SS, Tong W, et al. (2006) Mitochondrial disease activates transcripts of the unfolded protein response and cell cycle and inhibits vesicular secretion and oligodendrocyte-specific transcripts. Mitochondrion 6: 161–175.
20. Schmidt O, Pfanner N, Meisinger C (2010) Mitochondrial protein import: from proteomics to functional mechanisms. Nat Rev Mol Cell Biol 11: 655–667.
21. Gerard B, Bourgeron T, Chretien D, Rotig A, Munnich A, et al. (1993) Uridine preserves the expression of respiratory enzyme deficiencies in cultured fibroblasts. Eur J Pediatr 152: 270.
22. Chaiyarit S, Thongboonkerd V (2009) Comparative analyses of cell disruption methods for mitochondrial isolation in high-throughput proteomics study. Anal Biochem 394: 249–258.
23. Laemmli UK (1970) Cleavage of structural proteins during the assembly of the head of bacteriophage T4. Nature 227: 680–685.
24. Bradford MM (1976) A rapid and sensitive method for the quantitation of microgram quantities of protein utilizing the principle of protein-dye binding. Anal Biochem 72: 248–254.
25. Storey ADaJD (2014) Q-value estimation for false discovery rate control. 1.38.0 ed.
26. Strimmer BKaK (2012) Estimation of (Local) False Discovery Rates and Higher Criticism. 1.2.10 ed.
27. Phasukkijwatana N, Kunhapan B, Stankovich J, Chuenkongkaew WL, Thomson R, et al. (2010) Genome-wide linkage scan and association study of PARL to the expression of LHON families in Thailand. Hum Genet 128: 39–49.
28. Singer KH, Scearce RM, Tuck DT, Whichard LP, Denning SM, et al. (1989) Removal of fibroblasts from human epithelial cell cultures with use of a complement fixing monoclonal antibody reactive with human fibroblasts and monocytes/macrophages. J Invest Dermatol 92: 166–170.
29. Smith AC, Blackshaw JA, Robinson AJ (2012) MitoMiner: a data warehouse for mitochondrial proteomics data. Nucleic Acids Res 40: D1160–1167.
30. Lane L, Argoud-Puy G, Britan A, Cusin I, Duek PD, et al. (2012) neXtProt: a knowledge platform for human proteins. Nucleic Acids Res 40: D76–83.
31. Tamura Y, Itoh K, Sesaki H (2011) SnapShot: Mitochondrial dynamics. Cell 145: 1158, 1158 e1151.
32. Meissner C, Lorenz H, Weihofen A, Selkoe DJ, Lemberg MK (2011) The mitochondrial intramembrane protease PARL cleaves human Pink1 to regulate Pink1 trafficking. J Neurochem 117: 856–867.
33. Jin SM, Youle RJ (2012) PINK1- and Parkin-mediated mitophagy at a glance. J Cell Sci 125: 795–799.
34. Bunai K, Yamane K (2005) Effectiveness and limitation of two-dimensional gel electrophoresis in bacterial membrane protein proteomics and perspectives. J Chromatogr B Analyt Technol Biomed Life Sci 815: 227–236.
35. Rabilloud T, Strub JM, Carte N, Luche S, Van Dorsselaer A, et al. (2002) Comparative proteomics as a new tool for exploring human mitochondrial tRNA disorders. Biochemistry 41: 144–150.
36. Ferreira R, Rocha H, Almeida V, Padrao AI, Santa C, et al. (2013) Mitochondria proteome profiling: a comparative analysis between gel- and gel-free approaches. Talanta 115: 277–283.
37. Carelli V, Rugolo M, Sgarbi G, Ghelli A, Zanna C, et al. (2004) Bioenergetics shapes cellular death pathways in Leber's hereditary optic neuropathy: a model of mitochondrial neurodegeneration. Biochim Biophys Acta 1658: 172–179.
38. Brown MD, Trounce IA, Jun AS, Allen JC, Wallace DC (2000) Functional analysis of lymphoblast and cybrid mitochondria containing the 3460, 11778, or 14484 Leber's hereditary optic neuropathy mitochondrial DNA mutation. J Biol Chem 275: 39831–39836.
39. Giordano C, Iommarini L, Giordano L, Maresca A, Pisano A, et al. (2014) Efficient mitochondrial biogenesis drives incomplete penetrance in Leber's hereditary optic neuropathy. Brain 137: 335–353.
40. Qian Y, Zhou X, Liang M, Qu J, Guan MX (2011) The altered activity of complex III may contribute to the high penetrance of Leber's hereditary optic neuropathy in a Chinese family carrying the ND4 G11778A mutation. Mitochondrion 11: 871–877.
41. Watmough NJ, Frerman FE (2010) The electron transfer flavoprotein: ubiquinone oxidoreductases. Biochim Biophys Acta 1797: 1910–1916.
42. Chevrollier A, Guillet V, Loiseau D, Gueguen N, de Crescenzo MA, et al. (2008) Hereditary optic neuropathies share a common mitochondrial coupling defect. Ann Neurol 63: 794–798.
43. Angebault C, Gueguen N, Desquiret-Dumas V, Chevrollier A, Guillet V, et al. (2011) Idebenone increases mitochondrial complex I activity in fibroblasts from LHON patients while producing contradictory effects on respiration. BMC Res Notes 4: 557.
44. Ostermann J, Horwich AL, Neupert W, Hartl FU (1989) Protein folding in mitochondria requires complex formation with hsp60 and ATP hydrolysis. Nature 341: 125–130.
45. Magen D, Georgopoulos C, Bross P, Ang D, Segev Y, et al. (2008) Mitochondrial hsp60 chaperonopathy causes an autosomal-recessive neurodegenerative disorder linked to brain hypomyelination and leukodystrophy. Am J Hum Genet 83: 30–42.
46. Hansen JJ, Durr A, Cournu-Rebeix I, Georgopoulos C, Ang D, et al. (2002) Hereditary spastic paraplegia SPG13 is associated with a mutation in the gene encoding the mitochondrial chaperonin Hsp60. Am J Hum Genet 70: 1328–1332.
47. Hansen J, Svenstrup K, Ang D, Nielsen MN, Christensen JH, et al. (2007) A novel mutation in the HSPD1 gene in a patient with hereditary spastic paraplegia. J Neurol 254: 897–900.
48. Ali YO, Kitay BM, Zhai RG (2010) Dealing with misfolded proteins: examining the neuroprotective role of molecular chaperones in neurodegeneration. Molecules 15: 6859–6887.
49. Bini L, Magi B, Marzocchi B, Arcuri F, Tripodi S, et al. (1997) Protein expression profiles in human breast ductal carcinoma and histologically normal tissue. Electrophoresis 18: 2832–2841.
50. Bender T, Lewrenz I, Franken S, Baitzel C, Voos W (2011) Mitochondrial enzymes are protected from stress-induced aggregation by mitochondrial chaperones and the Pim1/LON protease. Mol Biol Cell 22: 541–554.
51. Mootha VK, Lepage P, Miller K, Bunkenborg J, Reich M, et al. (2003) Identification of a gene causing human cytochrome c oxidase deficiency by integrative genomics. Proc Natl Acad Sci U S A 100: 605–610.
52. Gohil VM, Nilsson R, Belcher-Timme CA, Luo B, Root DE, et al. (2010) Mitochondrial and nuclear genomic responses to loss of LRPPRC expression. J Biol Chem 285: 13742–13747.
53. Lu B, Yadav S, Shah PG, Liu T, Tian B, et al. (2007) Roles for the human ATP-dependent Lon protease in mitochondrial DNA maintenance. J Biol Chem 282: 17363–17374.
54. Aebi H (1984) Catalase in vitro. Methods Enzymol 105: 121–126.
55. Radi R, Turrens JF, Chang LY, Bush KM, Crapo JD, et al. (1991) Detection of catalase in rat heart mitochondria. J Biol Chem 266: 22028–22034.
56. Radi R, Sims S, Cassina A, Turrens JF (1993) Roles of catalase and cytochrome c in hydroperoxide-dependent lipid peroxidation and chemiluminescence in rat heart and kidney mitochondria. Free Radic Biol Med 15: 653–659.
57. Bai J, Cederbaum AI (2001) Mitochondrial catalase and oxidative injury. Biol Signals Recept 10: 189–199.
58. Van Laar VS, Dukes AA, Cascio M, Hastings TG (2008) Proteomic analysis of rat brain mitochondria following exposure to dopamine quinone: implications for Parkinson disease. Neurobiol Dis 29: 477–489.
59. Burte F, De Girolamo LA, Hargreaves AJ, Billett EE (2011) Alterations in the mitochondrial proteome of neuroblastoma cells in response to complex 1 inhibition. J Proteome Res 10: 1974–1986.
60. Whitfield ML, Finlay DR, Murray JI, Troyanskaya OG, Chi JT, et al. (2003) Systemic and cell type-specific gene expression patterns in scleroderma skin. Proc Natl Acad Sci U S A 100: 12319–12324.
61. Phasukkijwatana N, Chuenkongkaew WL, Suphavilai R, Suktitipat B, Pingsuthiwong S, et al. (2006) The unique characteristics of Thai Leber hereditary optic neuropathy: analysis of 30 G11778A pedigrees. J Hum Genet 51: 298–304.
62. Pejznochova M, Tesarova M, Honzik T, Hansikova H, Magner M, et al. (2008) The developmental changes in mitochondrial DNA content per cell in human cord blood leukocytes during gestation. Physiol Res 57: 947–955.
63. Caldas J, Gehlenborg N, Kettunen E, Faisal A, Ronty M, et al. (2012) Data-driven information retrieval in heterogeneous collections of transcriptomics data links SIM2s to malignant pleural mesothelioma. Bioinformatics 28: 246–253.

OPEN

Citation: Oncogenesis (2014) 3, e94; doi:10.1038/oncsis.2014.6

www.nature.com/oncsis

ORIGINAL ARTICLE

Lamin B2 prevents chromosome instability by ensuring proper mitotic chromosome segregation

T Kuga[1,2,3], H Nie[2], T Kazami[2], M Satoh[2], K Matsushita[2], F Nomura[2], K Maeshima[4], Y Nakayama[3] and T Tomonaga[1,2]

The majority of human cancer shows chromosomal instability (CIN). Although the precise mechanism remains largely uncertain, proper progression of mitosis is crucial. B-type lamins were suggested to be components of the spindle matrix of mitotic cells and to be involved in mitotic spindle assembly; thus, B-type lamins may contribute to the maintenance of chromosome integrity. Here, using a proteomic approach, we identified lamin B2 as a novel protein involved in CIN. Lamin B2 expression decreased in colorectal cancer cell lines exhibiting CIN, as compared with colorectal cancer cell lines exhibiting microsatellite instability (MIN), which is mutually exclusive to CIN. Importantly, lamin B2 knockdown in MIN-type colorectal cancer cells induced CIN phenotypes such as aneuploidy, chromosome mis-segregation and aberrant spindle assembly, whereas ectopic expression of lamin B2 in CIN-type colorectal cancer cells prevented their CIN phenotypes. Additionally, immunohistochemical analysis showed a lower expression of lamin B2 in cancer tissues extracted from patients with sporadic colorectal cancer (CIN-type) than that from patients with hereditary non-polyposis colorectal cancer (HNPCC; MIN type). Intriguingly, mitotic lamin B2 in MIN cancer cells was localized outside the spindle poles and mitotic lamin B2 localization was diminished in CIN cancer cells, suggesting an important role of lamin B2 in proper mitotic spindle formation. The obtained results suggest that lamin B2 maintains chromosome integrity by ensuring proper spindle assembly and that its downregulation causes CIN in colorectal cancer.

Oncogenesis (2014) **3,** e94; doi:10.1038/oncsis.2014.6; published online 17 March 2014

Subject Categories: Molecular oncology

Keywords: colorectal cancer; chromosomal instability; lamin B2; chromosome segregation; mitotic spindle

INTRODUCTION

Cancer is widely accepted as a disease of genetic instability. This instability exists as two distinct forms: chromosomal instability (CIN), characterized by gains or losses of whole or large portions of chromosomes, and microsatellite instability (MIN), characterized by mutations at the nucleotide level.[1–3] The fact that most cancers have abnormal chromosomal content, called aneuploidy, indicates that CIN has an important role in carcinogenesis.[4]

CIN has been recognized to occur as a result of chromosome mis-segregation, which is caused by defects in mitotic functions, such as chromosome condensation, sister-chromatid cohesion, kinetochore structure, centrosome formation and microtubule dynamics, as well as the mitotic checkpoint that monitors the proper progression of mitosis.[4] Several proteins involved in mitotic processes have been shown to have mutated or altered expression levels in cancer.[5–8] Moreover, we previously showed that core kinetochore proteins, CENP-A and CENP-H, are overexpressed in colorectal cancer and involved in CIN,[9–11] suggesting that nuclear proteins are also responsible for chromosome integrity.

Nuclear lamins were initially identified as the major components of the nuclear lamina, a proteinaceous layer found at the interface between chromatin and inner nuclear membrane.[12] Although the early view of lamins was as a static nuclear skeleton, recent observations suggest that lamins have far more active roles throughout the cell cycle, such as DNA replication, transcription and several mitotic events.[13–23] Lamins are grouped as A type (lamins A and C) or B type (lamins B1 and B2) on the basis of their biochemical properties and behavior during mitosis.[24] B-type lamins are expressed in all somatic cell types, whereas A-type lamins are expressed primarily in differentiated cells.[24]

During mitosis, B-type lamin has been observed to associate with the mitotic spindle[25,26] and shown to have an important role in mitotic spindle formation.[14,21] Both depletion and a dominant-negative mutant of lamin B proteins disrupted spindle assembly in mitosis.[21] In *C. elegans*, downregulation of lamin expression induced gross mitotic defects, such as anaphase chromosome 'bridges' and unequal distribution of chromatin to daughter cells.[13] These observations suggest that B-type lamins have an important role in proper chromosome segregation.

In this study, we searched for CIN-related proteins using a proteomic approach and showed the important role of lamin B2 in CIN by manipulating its expression levels in CIN and MIN colorectal cancer cell lines. Moreover, we observed a decreased expression of lamin B2 in human sporadic colorectal cancer tissues (CIN type) as compared with hereditary non-polyposis colorectal cancer tissues (HNPCC, MIN type). Additionally, by dissecting mitotic localization of lamin B2, we suggested a novel mechanism of how lamin B2 maintains mitotic spindle assembly to prevent CIN.

[1]Laboratory of Proteome Research, National Institute of Biomedical Innovation, Osaka, Japan; [2]Department of Molecular Diagnosis (F8), Graduate School of Medicine, Chiba University, Chiba, Japan; [3]Department of Biochemistry and Molecular Biology, Kyoto Pharmaceutical University, Kyoto, Japan and [4]Biological Macromolecules Laboratory, Structural Biology Center, National Institute of Genetics, Shizuoka, Japan. Correspondence: Professor T Tomonaga, Laboratory of Proteome Research, National Institute of Biomedical Innovation, 7-6-8 Saito-Asagi, Ibaraki567-0085, Osaka, Japan.
E-mail: tomonaga@nibio.go.jp
Received 25 May 2013; revised 27 December 2013; accepted 27 January 2014

RESULTS

Proteomic analysis of colorectal cancer cell lines reveals that lamin B2 is downregulated in CIN cell lines

To search for the factors involved in CIN, we compared protein expression profiles of CIN and MIN colorectal cancer cell lines by a proteomic approach. Both types of cell lines have previously been well studied;[1,27] thus, we used HT29, SW480, SW837 and Caco-2 as CIN cell lines and HCT116, RKO, DLD1 and SW48 as MIN cell lines. Nuclear proteins were extracted from each cell line. Pooled nuclear extracts of CIN cell lines were labeled with Cy5 dyes, whereas those of MIN cell lines were labeled with Cy3 dyes. The labeled proteins were mixed and separated in the same agarose two-dimensional electrophoresis gel (Figure 1a). Proteins that increased or decreased in CIN nuclear extracts (displayed as red or green spots, respectively) were identified by tandem mass spectrometry and their expression levels were validated by western blotting.

One of the clearest differences in expression between CIN and MIN nuclear extracts was that of lamin B2, which significantly decreased in all tested CIN cell lines as compared with MIN cell lines (Figures 1a, arrow and b). In contrast, lamin B1 did not show a clear difference between CIN and MIN cell lines, and the expression of lamin A/C varied between individual cell lines (Figure 1b). Immunofluorescence for lamin B2 further confirmed the decreased level of lamin B2 in CIN cell lines. Although strong lamin B2 staining was detected at the nuclear envelope in several MIN cell lines, the staining was very slight in CIN cell lines (Figure 1c). Thus, these results indicate that the expression of lamin B2 is specifically suppressed in CIN cell lines.

Repression of lamin B2 in MIN cancer cells causes aneuploidy

To examine whether the decreased expression of lamin B2 was involved in CIN, MIN-type HCT116 cells were transfected with lamin B2-siRNA and analyzed for alterations in the chromosome number by fluorescent in situ hybridization (FISH) analysis using several centromere probes (CEPs). Depletion of lamin B2 was checked by western blotting (Figure 2a, lanes 1 and 2) and reverse transcription (RT)–PCR (Supplementary Figure S1). Figure 2b shows that lamin B2 knockdown increased the number of aneuploid cells (arrows). As assessed by counting the number of centromere signals for chromosomes 7, 8, 12 and 15 in at least 200 nuclei, the frequency of aneuploid cells increased 2.2–4.4 times in lamin B2-siRNA-treated cells as compared with control cells (Figure 2c). Similar results were obtained using another lamin B2-siRNA targeting a different region of lamin B2 mRNA (Supplementary Figure S2).

To exclude the possibility that the aneuploidy observed above was due to the off-target effect of lamin B2-siRNA, HCT116 cells were co-transfected with lamin B2-siRNA and lamin B2-GFP plasmid, which would replace the expression and function of endogenous lamin B2. The expression level of lamin B2-GFP was comparable to that of endogenous lamin B2 (Figure 2a). The number of aneuploid cells was then evaluated. By transfection with lamin B2-GFP, the frequency of aneuploidy was markedly decreased as compared with that in cells treated with lamin B2-siRNA alone, and it was almost comparable to that of control-siRNA-treated cells (Figure 2c). These results indicate that the suppression of lamin B2 causes aneuploidy.

To examine the effect of lamin B2 stable knockdown on the proliferation and CIN of cancer cells, we attempted to generate HCT116 MIN cell lines stably depleted of lamin B2 using four plasmids encoding different lamin B2-shRNA. We could obtain only one clone exhibiting ~60–70% depletion of lamin B2 (Supplementary Figure S3a). This clone showed neither increased frequency of aneuploidy (Supplementary Figure S3b) nor alteration in cell proliferation (data not shown). These results suggest that this incomplete depletion of lamin B2 may not be satisfactory to cause CIN, and that a certain level of lamin B2 is sufficient to maintain chromosome integrity. Because MIN cell lines maintain the checkpoint system against aneuploidy,[28] HCT116 cells depleted of lamin B2 at sufficient levels to cause CIN might be lost by cell death or cell-cycle arrest during the clonal selection. Further study using other approaches is also needed to understand the effects of CIN caused by lamin B2 depletion on cancer survival.

Repression of lamin B2 in MIN cancer cells causes mitotic delay and chromosome mis-segregation

To further examine whether the aneuploidy observed by the depletion of lamin B2 occurred as the result of chromosome mis-segregation, HCT116 cells expressing histone H2B-GFP were treated with lamin B2-siRNA and live-cell imaging of the mitosis was carried out. The duration of mitosis in lamin B2-siRNA-treated cells was significantly longer than in control cells. Compared with control cells that took 12.5 ± 5.6 min from congression to separation of sister chromatids, lamin B2-siRNA-treated cells took more than two times longer (28.9 ± 18.2 min; Student's *t*-test; $P = 2 \times 10^{-12}$) to complete metaphase (Figure 2d; Supplementary Figure S4; Supplementary Videos 1 and 2). Moreover, lamin B2-depleted cells often showed signs of chromosome mis-segregation, such as chromosome bridges and lagging chromosomes (Figure 2d, arrowheads). These results strongly suggest that lamin B2 is involved in proper chromosome segregation.

Repression of lamin B2 in MIN cancer cells compromises mitotic spindle formation

What is the mechanism of the aberrant mitosis induced by suppression of lamin B2 expression? Recent reports showed that B-type lamins are required for spindle assembly;[14,21] thus, to test the hypothesis that suppression of lamin B2 in MIN cancer cells induces abnormal spindle assembly, two MIN cell lines, HCT116 and RKO, were transfected with lamin B2-siRNA and examined by immunofluorescence with antibodies against α- and β-tubulin, components of the mitotic spindle. For accumulation of mitotic cells, 48 h after transfection, cells were synchronized with thymidine for 16 h and then cultured in fresh medium for 10–12 h. Depletion of lamin B2 caused a spindle defect or poor spindle morphology with a lack of chromosome congression, whereas control cells showed clear mitotic spindles (Figures 3a and b). Suppression of lamin B2 in HCT116 cells caused an increase in the spindle defect to 40.6% as compared with 16.0% of control cells ($n = 50$–100 mitotic cells). These results suggest that depletion of lamin B2 induces mitotic defects, mainly due to aberrant spindle assembly.

Ectopic expression of lamin B2 in CIN cancer cells prevents chromosome mis-segregation and severe aneuploidy

We next examined whether the induction of lamin B2 expression in CIN cancer cells could rescue the mitotic defects characteristic of CIN. CIN-type WiDr cells expressing histone H2B-GFP were transfected with lamin B2-mCherry and live-cell imaging of mitosis was carried out. Expression of lamin B2-mCherry was confirmed by western blotting (Figure 4a) and fluorescence microscopy (Figure 4b). Cells transfected with the control plasmid encoding mCherry alone exhibited chromosome bridges or lagging chromosomes in anaphase at high frequency (38.1%) (Figure 4b; Supplementary Video 3). In addition, these cells showed severe mitotic delay, 166 ± 125 min from nuclear envelope breakdown to anaphase onset (Figure 4c). Strikingly, ectopic expression of lamin B2-mCherry not only decreased the frequency of anaphase chromosome mis-segregation (24.4%) but significantly improved mitotic delay (75 ± 24 min) (Figures 4b and c; Supplementary Video 4). These results suggest that lamin B2 re-expression promotes accurate chromosome congression and prevents chromosome mis-segregation.

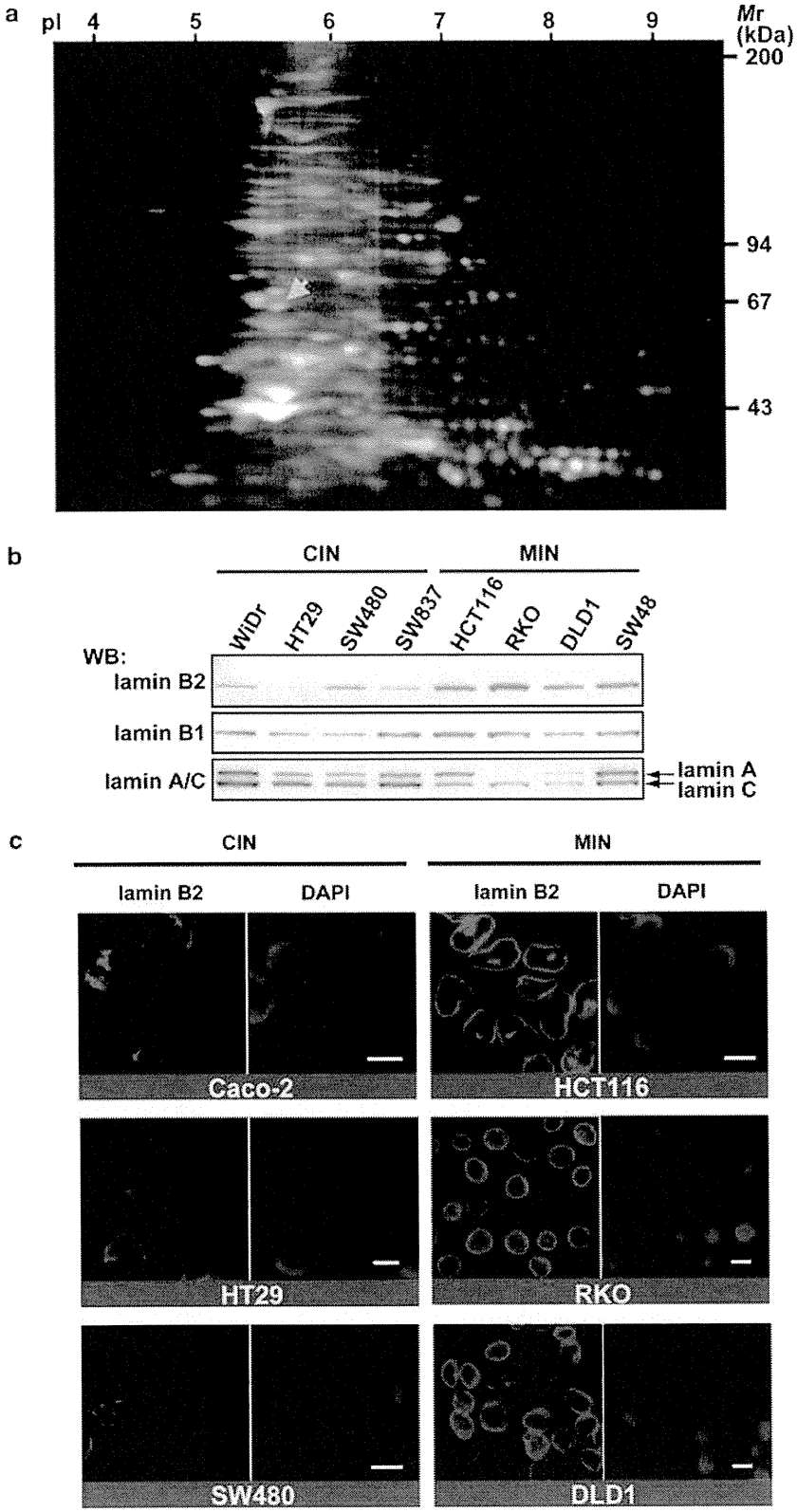

Figure 1. Proteomic analysis of colorectal cancer cell lines revealed that lamin B2 is downregulated in CIN cell lines. (**a**) Proteomic analysis of CIN and MIN cell lines using agarose 2D-DIGE. Nuclear extracts prepared from the cell lines were labeled with Cy3 (MIN) and Cy5 (CIN), and separated with two-dimensional electrophoresis. Increased and decreased protein spots in CIN nuclei are displayed as red (Cy5) and green (Cy3), respectively. Yellow arrow shows the protein spot corresponding to lamin B2. (**b**) Western blot analysis of nuclear extracts (10 μg) from CIN and MIN cell lines using antibodies to lamin B2, B1 and lamin A/C. (**c**) Immunostaining of CIN and MIN cell lines using anti-lamin B2 antibody and DAPI for DNA. Images show interphase cells. Scale bars, 10 μm.

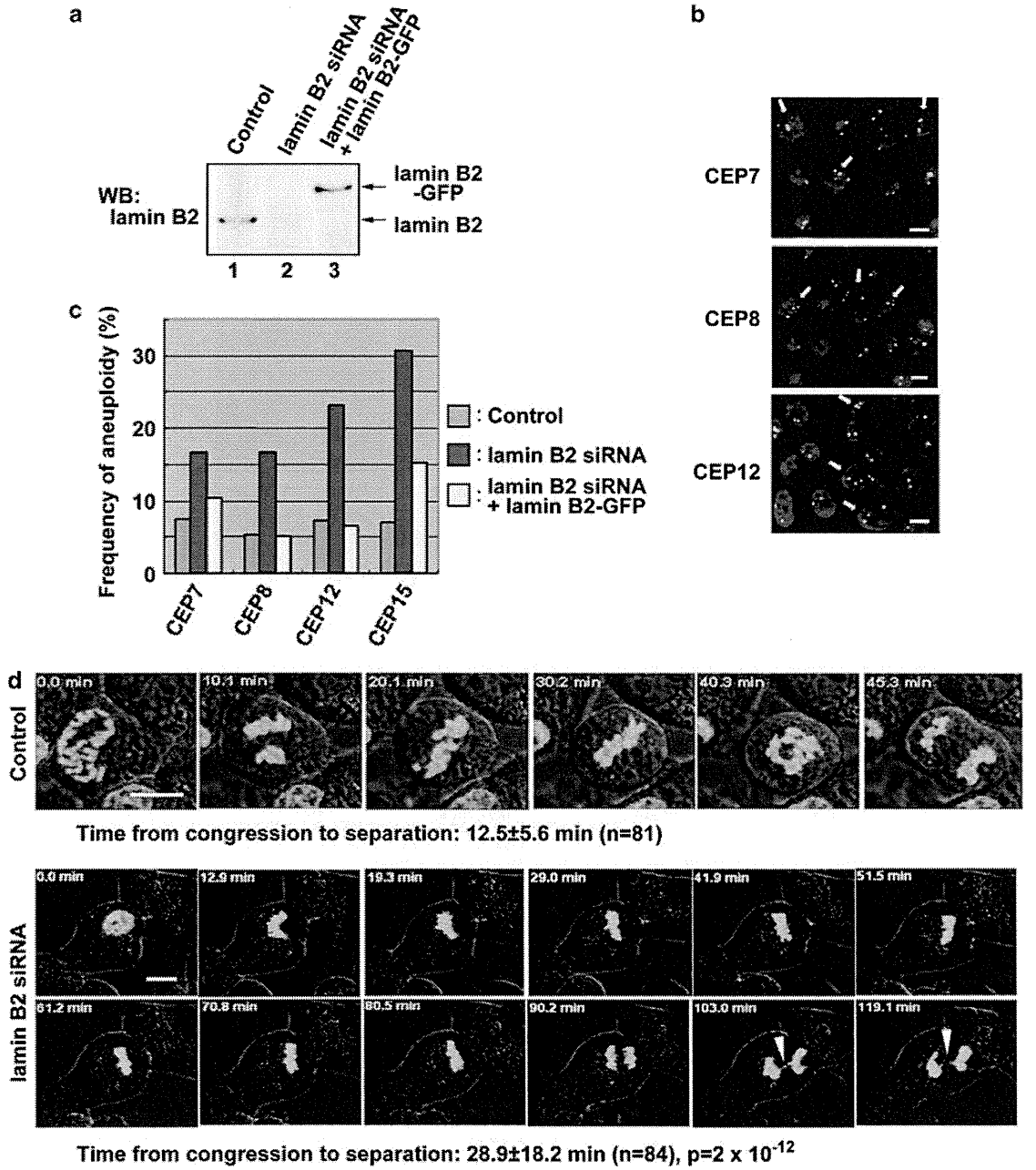

Figure 2. Repression of lamin B2 induces mitotic defects and aneuploidy. (**a**) Lamin B2-siRNA alone or together with lamin B2-GFP expression plasmid was transfected into MIN-type HCT116 cells and, 48 h later, the expressions of lamin B2 and lamin B2-GFP were checked by western blotting. Lane 1, control-siRNA; lane 2, lamin B2-siRNA alone; lane 3, lamin B2-siRNA + lamin B2-GFP expression plasmid. (**b**) FISH analysis using centromere probes (CEP7, 8 and 12) was performed 48 h after transfection with lamin B2-siRNA in HCT116 cells. White arrows indicate aneuploid cells. (**c**) Frequency of aneuploid cells in HCT116 cells transfected with either lamin B2-siRNA alone or together with lamin B2-GFP expression plasmid. Centromere singles (CEP7, 8, 12 and 15) were counted in at least 200 cells. (**d**) HCT116 cells stably expressing histone H2B-GFP were treated with control or lamin B2-siRNA for 24 h. Time-lapse images of the cells were taken at 3- to 5-min intervals. Images shown are representative of control or lamin B2-siRNA-treated cells from prophase to anaphase. Control cells took 12.5 ± 5.6 min ($n = 81$) from congression to separation of sister chromatids, whereas lamin B2-siRNA-treated cells took 28.9 ± 18.2 min ($n = 84$). Arrowheads indicate a chromosomal bridge. Scale bars, 10 μm.

We next examined aneuploidy in lamin B2-overexpressed CIN cells. WiDr cells were transfected with lamin B2-GFP or GFP alone (control) and, 7 days after transfection, analyzed by FISH with CEP12 and 15. A large fraction of control cells exhibited three copies of CEP12 and 15 signals, whereas 9.5 ± 1.5% and 14.5 ± 2.5% of control cells exhibited ⩾4 copies of CEP12 and 15 signals, respectively (Figures 4d and e). Strikingly, ectopic expression of lamin B2-GFP decreased the number of severely aneuploid cells exhibiting ⩾4 copies of CEP12 (6.0 ± 4.7%) and CEP15 (4.6 ± 1.5%) signals, while the number of cells exhibiting 3 copies of these CEP signals increased (Figures 4d and e). Given that intercellular heterogeneity in the chromosome copy number is a typical feature of CIN cancer cells,[1,28] these results suggest that lamin B2 overexpression improves chromosome integrity.

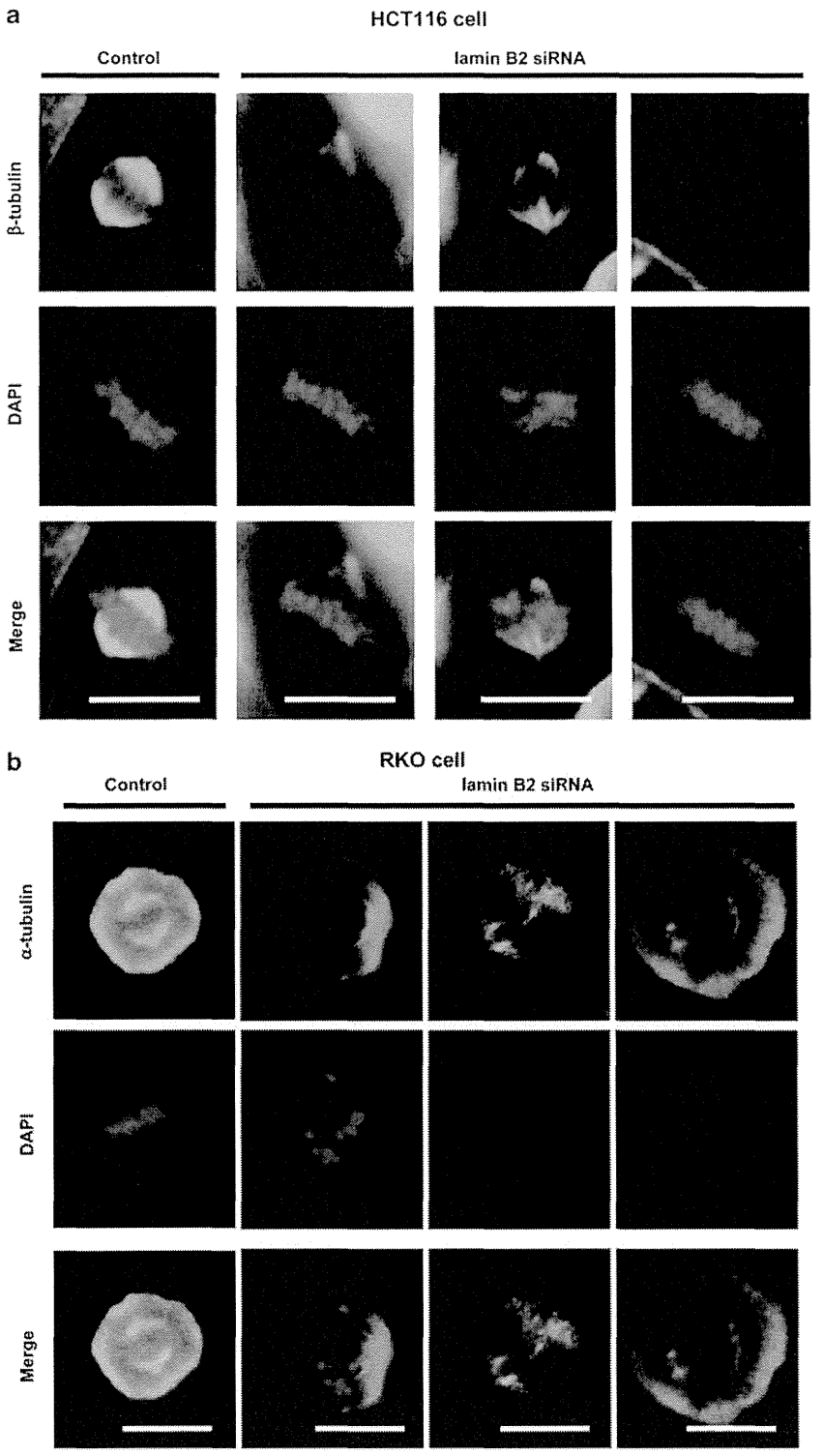

Figure 3. Repression of lamin B2 abrogates mitotic spindle formation. MIN cell lines, HCT116 and RKO, were transfected with control- or lamin B2-siRNA. Forty-eight hours after transfection, the cells were synchronized with thymidine for 16 h and then released into fresh medium. Cells that entered mitosis were analyzed by immunostaining using anti-β-tubulin (**a**) and α-tubulin (**b**) antibodies in HCT116 (**a**) and RKO (**b**) cells, respectively. DNA was marked by DAPI. Scale bars, 10 μm.

Ectopic expression of lamin B2 in CIN cancer cells prevents aberrant mitotic spindle formation

We further examined mitotic spindle formation in CIN cancer cells with overexpression of lamin B2. To monitor mitotic spindle formation, we generated WiDr cells stably expressing mCherry-α-tubulin. The cells were transfected with lamin B2-GFP or GFP (control) and live-cell imaging of mitosis was carried out. Control cells showed poor spindle morphology at high frequency (38.0%) during chromosome segregation (Figure 5; Supplementary Video 5), suggesting that mitotic spindle formation is disturbed

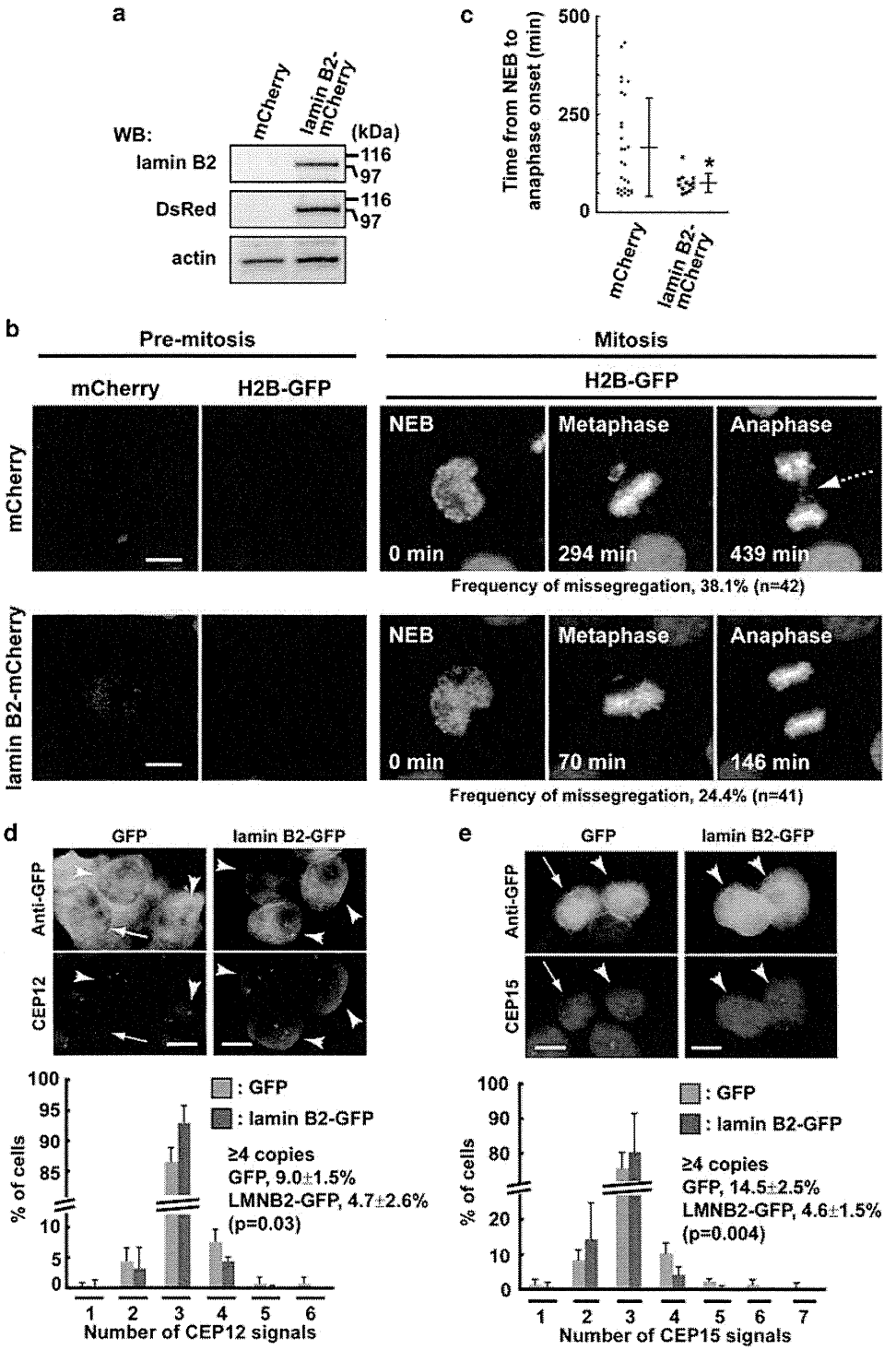

Figure 4. Ectopic expression of lamin B2 in CIN cancer cells prevents mitotic defects. (**a**–**c**) WiDr cells stably expressing histone H2B-GFP were transfected with lamin B2-mCherry or mCherry (control) expression plasmid, and expression of lamin B2-mCherry (M_r, 96 kDa) was examined by western blotting with anti-lamin B2 and anti-DsRed antibodies (**a**). Anti-DsRed antibody can detect mCherry. Living cells expressing lamin B2-mCherry or mCherry were monitored by confocal microscopy. Representative images of living cells are shown (**b**). Elapsed times from nuclear envelope breakdown (NEB) are indicated at the bottom of mitotic images (**b**). Dotted arrow indicates chromosome mis-segregation in anaphase. Scale bars, 10 μm. Percentages of cells exhibiting chromosome mis-segregation during anaphase (mCherry, $n=42$; lamin B2-mCherry, $n=41$) are indicated below mitotic images (**b**). (**c**) Plot represents the value of the time from NEB to anaphase onset in each cell, and the means ± s.d. are shown (mCherry, $n=28$; lamin B2-mCherry, $n=13$). Asterisk indicates a significant difference from the control, calculated by Student's *t*-test (*$P<0.05$). (**d**, **e**) CIN-type WiDr cells were transfected with lamin B2-GFP or GFP (control) expression plasmid. Seven days after transfection, cells were analyzed by immunofluorescence with anti-GFP antibody and FISH with CEP12 (**d**) or CEP15 (**e**). DNA was marked by DAPI. Projections of z-stack images at 1-μm intervals are shown. Arrowheads and arrows indicate cells exhibiting 3 and ⩾4 copies of CEP signals, respectively. Scale bars, 10 μm. Bar diagrams show percentages of cells exhibiting indicated copies of CEP12 (**d**) or CEP15 (**e**) signals. Data are the mean ± s.d. of four (**d**) or three (**e**) independent experiments ($n>100$ cells for each experiment). The percentage of cells exhibiting ⩾4 copies of CEP12 (**d**) or CEP15 (**e**) signals significantly decreased upon lamin B2 ectopic expression (Student's *t*-test).

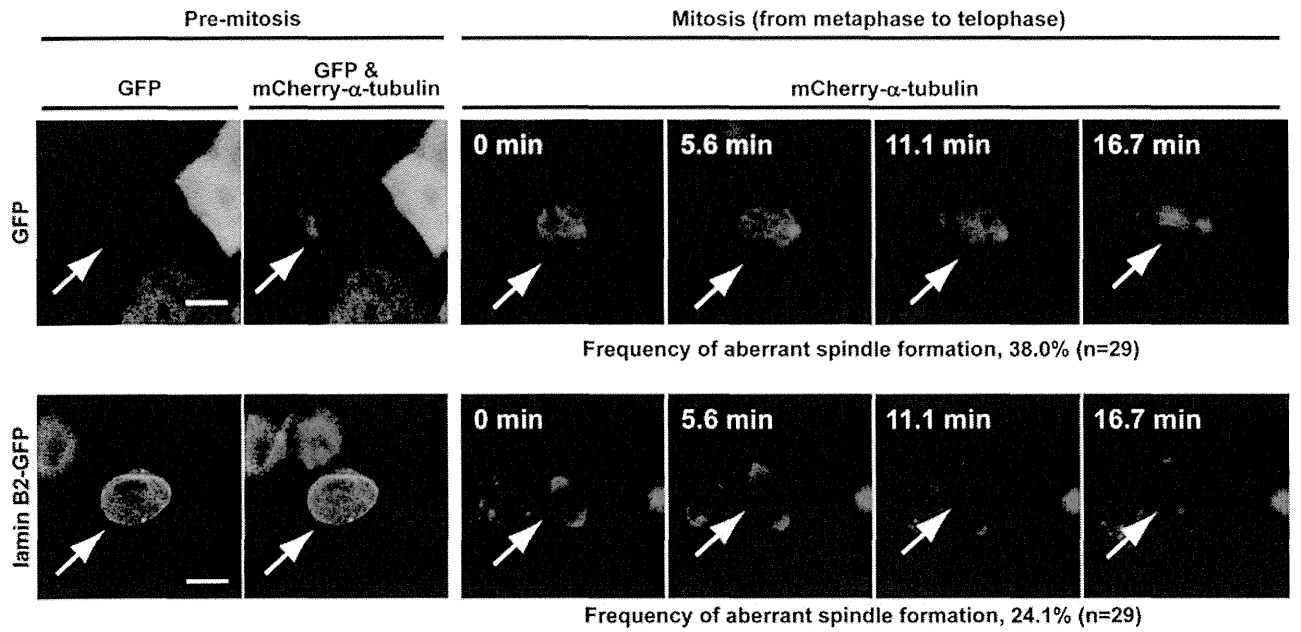

Figure 5. Ectopic expression of lamin B2 in CIN cancer cells prevents aberrant mitotic spindle formation. WiDr cells stably expressing mCherry-α-tubulin were transfected with lamin B2-GFP or GFP (control) expression plasmid. Living cells expressing lamin B2-GFP or GFP were monitored by confocal microscopy. Images shown are representative cells (arrows). Scale bars, 10 μm. Elapsed times during chromosome segregation are indicated at the top of mitotic images. Percentages of cells exhibiting aberrant spindle formation during mitosis (GFP, $n = 29$; lamin B2-GFP, $n = 29$) are indicated below mitotic images.

in WiDr cells. In lamin B2-GFP-expressing cells, the frequency of poor spindle morphology was reduced (24.1%) (Figure 5; Supplementary Video 6). These results suggest that lamin B2 overexpression improves the accuracy of chromosome segregation by preventing aberrant mitotic spindle formation.

Mitotic lamin B2 localization outside the spindle poles disappears in CIN cancer cells

Previous reports suggested that B-type lamins are structural components of the mitotic spindle matrix required to promote spindle assembly.[21] To visualize mitotic lamin B2 in CIN and MIN cell lines, we performed immunofluorescence with anti-lamin B2 antibody. Although HCT116 and DLD1 MIN lines exhibited intensive staining for mitotic lamin B2 around the spindle poles, SW837 and HT29 CIN lines showed no or very weak staining for mitotic lamin B2 (Figure 6a). These results suggest that CIN cancer cells largely lose the mitotic function of lamin B2.

Unexpectedly, lamin B2 in MIN colorectal cancer cell lines was distributed mainly outside the spindle poles (Figure 6a, magnified images), although the previous report showed co-localization of lamin B2 with kinetochore microtubules in mitotic HeLa cells.[21] Staining of mitotic lamin B2 in HCT116 MIN cells was detected using both rabbit (Figure 6a) and mouse (Figure 6b) anti-lamin B2 antibodies and disappeared upon treatment with lamin B2-siRNA (Figure 6b), confirming the specificity of mitotic lamin B2 staining. Lamin B1 was also localized outside spindle poles, but more broadly than lamin B2. Lamin A/C showed uniform staining throughout the cytoplasm (Figures 6c and d). The specificity of lamins B1 and A/C staining was also confirmed by their knockdown (Figures 6c and d). The mitotic lamin B3 matrix formed in Xenopus egg extracts contained spindle assembly factors, including Eg5[21]; however, in HCT116 cells, a large fraction of lamin B2 was not co-localized with Eg5 (Figure 6e). Taken together, these results suggest that the disappearance of mitotic lamin B2 outside the spindle poles is involved in aberrant spindle assembly and chromosome mis-segregation.

SUN1 is a protein associated with mitotic lamin B2

To further understand the role of lamin B2 in spindle formation, we identified proteins associated with lamin B2 in mitosis. Immunoprecipitates using anti-lamin B2, B1 or A/C antibody were prepared from mitotic HCT116 MIN cells and analyzed by LC-MS/MS. By comparing proteins identified from lamin B2 immunoprecipitates with those of lamin B1 and A/C immunoprecipitates, SUN1, an inner nuclear membrane protein,[29,30] was determined as a mitotic lamin B2-associated protein (Supplementary Table S1). In mitotic HCT116 cells, SUN1 was colocalized with lamin B2 and SUN1 staining was attenuated upon knockdown of SUN1 (Figure 6f), indicating that SUN1 is associated with mitotic lamin B2 outside the spindle poles. Since lamins and SUN1 were reported to be involved in stabilizing the position of the nucleus in the cell,[31,32] these results suggest that lamin B2 and SUN1 may contribute to mitotic spindle formation by physically supporting the spindle poles.

Sporadic colorectal cancer tissues (CIN) show decreased lamin B2 expression

The majority of human sporadic colorectal cancer exhibits CIN, whereas HNPCC exhibits MIN.[33] We therefore compared the lamin B2 expression in sporadic colorectal cancer tissues with that in HNPCC tissues. HNPCC patients were diagnosed based on Amsterdam criteria II, and paraffin-embedded tissues from sporadic colorectal cancers and HNPCCs were analyzed by immunohistochemistry with anti-lamin B2 antibody. The staining intensity of lamin B2 is objectively quantified using the TissueFAXS system and the corresponding HistoQuest software (TissueGnostics, Vienna, Austria). Sporadic colorectal cancer tissues showed lower levels of lamin B2 staining than HNPCC (Figures 7a and b; Table 1; Supplementary Figure S5), which supports the idea that repression of lamin B2 is involved in CIN. Interestingly, these data also showed that the mean intensity of lamin B2 expression in HNPCC (MIN) was 1.3 ± 0.4-hold higher than that in adjacent non-tumor tissues (Student's paired *t*-test, $P = 0.055$). These results suggest not only that a decrease in lamin B2 expression is involved in the induction

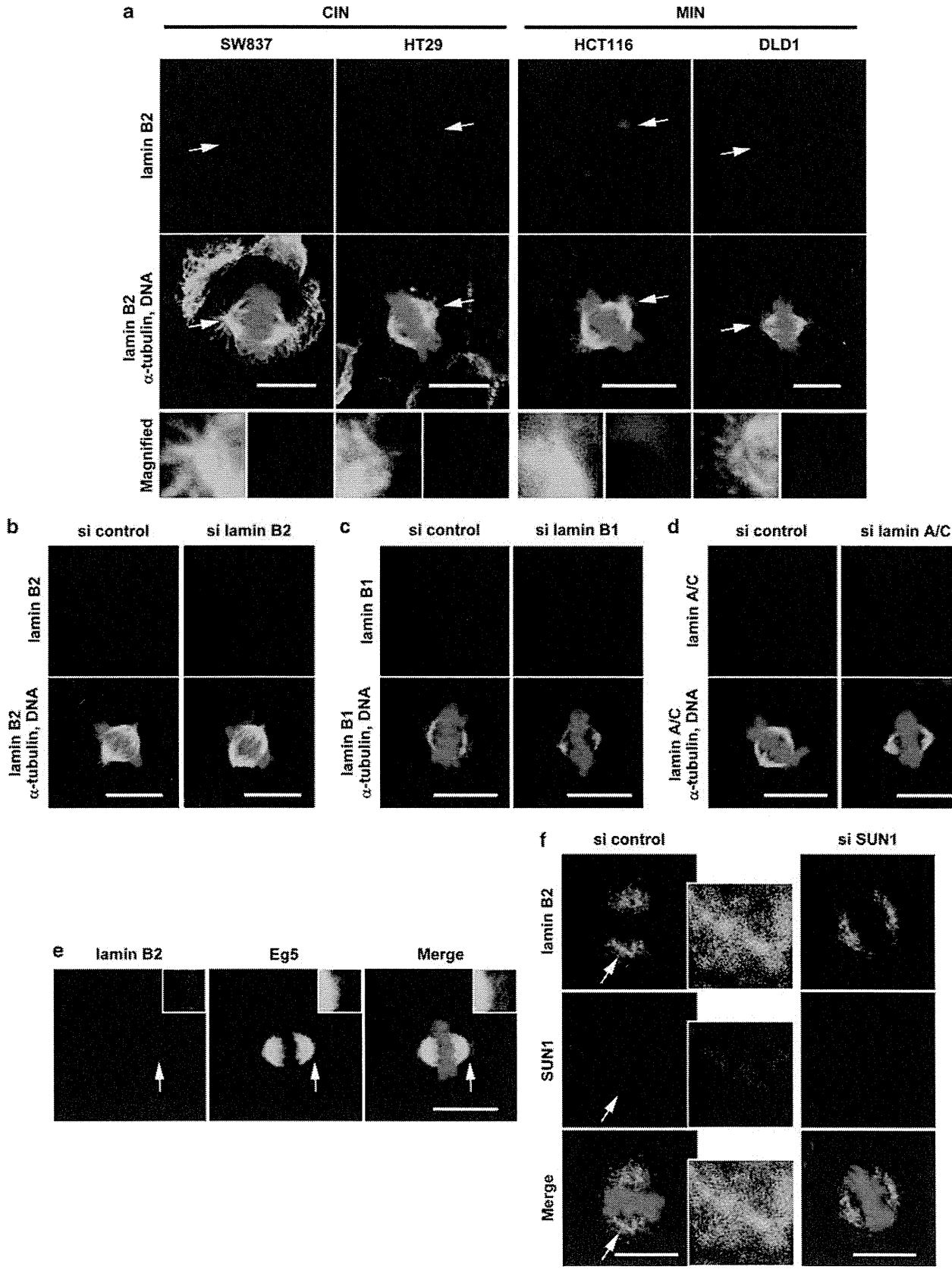

Figure 6. Disappearance of immunostaining for mitotic lamin B2 in CIN cell lines. (**a**) CIN (SW837 and HT29) and MIN (HCT116 and DLD1) cell lines were stained with anti-lamin B2 (red) and anti-α-tubulin (green) antibodies. Images show mitotic cells. (**b**–**d**, **f**) HCT116 cells were treated with siRNA targeting lamin B2 (**b**), B1(**c**) or A/C (**d**) or SUN1 (**f**) and stained with the indicated antibodies. (**e**) HCT116 cells were stained with anti-lamin B2 and anti-Eg5 antibodies. DNA was stained with DAPI (blue). Scale bars, 10 μm. The areas indicated by arrows are shown at high magnification.

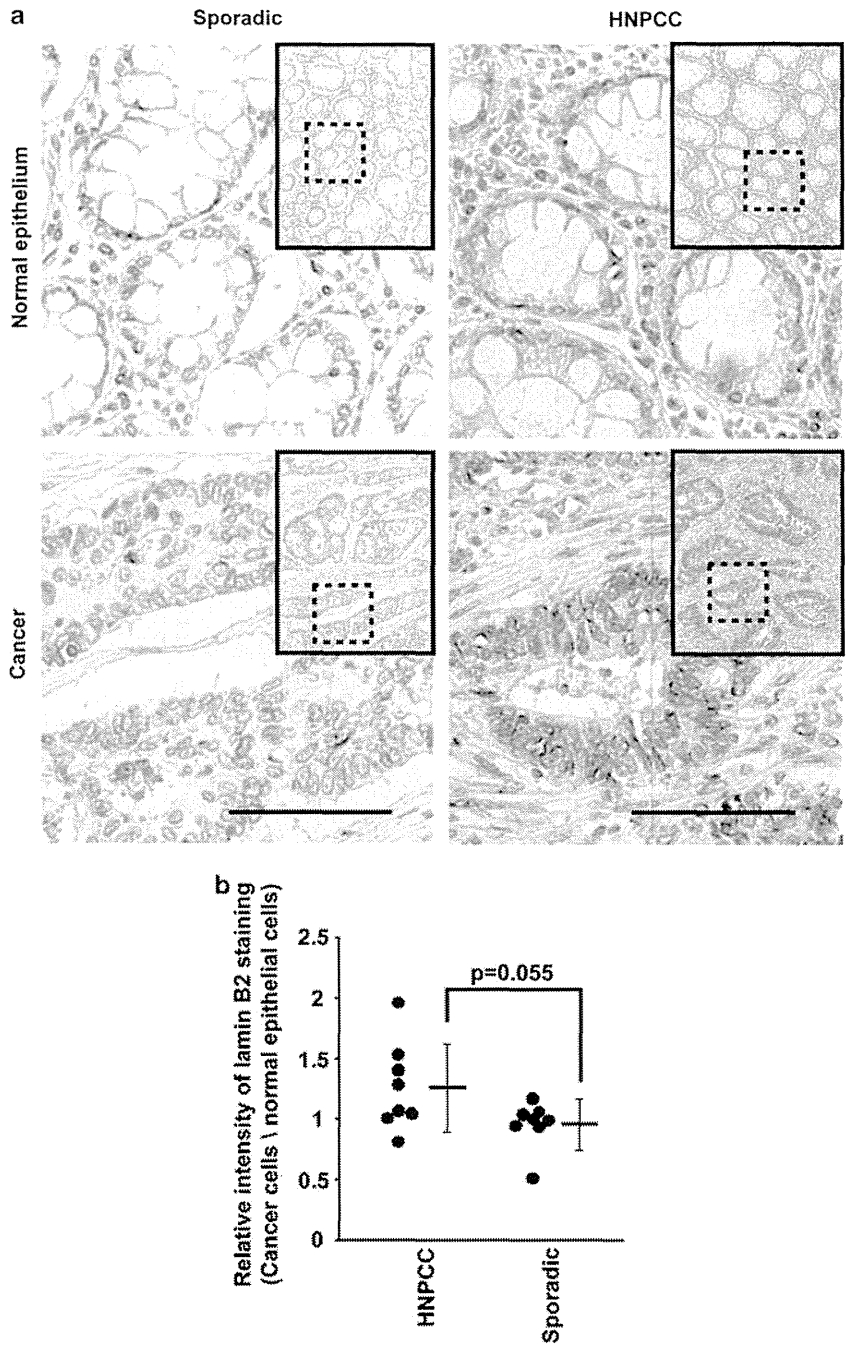

Figure 7. Immunohistochemical analysis of lamin B2 in sporadic colorectal cancer and HNPCC. Paraffin-embedded tissue sections of sporadic colorectal cancer (CIN) and HNPCC (MIN) were stained with rabbit polyclonal anti-lamin B2 antibody. Using the TissueFAXS system and HistoQuest software, images of cancer cells and adjacent normal epithelial cells in each tissue section were obtained, and the intensity of lamin B2 staining in these cells was quantitated. (**a**) Representative images at low and high magnification of the dotted square regions are shown. Bars, 100 μm. (**b**) Plot represents the value of the relative intensity of lamin B2 staining in cancer cells in each tissue section compared with the intensity in adjacent normal epithelial cells in the same tissue section, and the means ± s.d. are shown (sporadic colorectal cancer, $n = 8$; HNPCC, $n = 8$). The *P*-value was calculated by Student's *t*-test.

of CIN in human colorectal cancer but also that its enhanced expression might be required for MIN cancer to prevent CIN.

DISCUSSION

In this study, we provided the first evidence that downregulation of lamin B2 is involved in chromosome instability and that restoration of the lamin B2 level is able to prevent mitotic defects. Importantly, low levels of lamin B2 expression were observed not only in CIN colorectal cancer cell lines but also in sporadic colorectal cancer tissues (CIN). Furthermore, we determined a novel mitotic localization of lamin B2 outside the spindle poles. Our data suggest that lamin B2 has a critical role in preventing CIN in colorectal cancer by maintaining spindle pole stability and consequent spindle assembly.

The major cause of CIN is believed to be chromosome mis-segregation. Proper formation of bipolar spindles is crucial for accurate segregation of chromosomes.[4] Recent studies suggested

Table 1. Clinical features of patients with colorectal cancer

	Cancer type	*Age*	*Sex*	*Location*[a]	*Histological stage*	*Lamin B2 level*[a]
1	HNPCC	49	Male	R	3	1.4***
2	HNPCC	44	Male	S	4	1.0
3	HNPCC	46	Male	R	1	1.5***
4	HNPCC	44	Male	T	3	2.0***, 1.0[b]
5	HNPCC	57	Female	A	3	1.3***
6	HNPCC	48	Female	R	3	1.0
7	HNPCC	61	Female	A	2	0.8***
8	Sporadic	67	Male	T	3	0.9*
9	Sporadic	82	Male	A	2	1.2*
10	Sporadic	56	Female	A	3	1.0
11	Sporadic	67	Female	C	3	0.5***
12	Sporadic	41	Female	A	4	0.9
13	Sporadic	60	Male	S	3	1.1
14	Sporadic	67	Male	D,S	4	1.0
15	Sporadic	82	Male	D	2	1.0

Abbreviations: A, ascending colon; C, cecum; D, descending colon; R, rectum; S, sigmoid colon; T, traverse colon. Asterisks indicate significant differences between cancer and normal epithelial cells, calculated by Student's *t*-test (*$P<0.05$; ***$P<0.001$). [a]Levels of lamin B2 expression in cancer cells are relative to the adjacent normal epithelial cells (see Supplementary Figure S5). [b]Two distinct tissues from the same patient were examined for lamin B2 expression.

that B-type lamins associate with the mitotic spindle[25,26] and have an active role in mitotic progression by promoting the formation of a spindle matrix.[14,21] Furthermore, downregulation of lamin expression in *C. elegans* induced chromosome mis-segregation.[13] Intriguingly, in CIN colorectal cancer cell lines, lamin B2, but not lamins B1 and A/C, was specifically downregulated (Figure 1). Knockdown experiments of MIN colorectal cancer cells showed that decreased expression of lamin B2 is sufficient to cause aberrant spindle formation, chromosome mis-segregation and aneuploidy (Figures 2 and 3). These results suggest that lamin B2 is a cause of CIN in colorectal cancer.

Mitotic lamin B2 in MIN colorectal cancer cell lines was detected outside spindle poles (Figure 6a), although the previous report suggested that B-type lamins were co-localized with kinetochore microtubules in HeLa cells.[21] Mitotic lamin B2 staining outside the spindle poles was carefully confirmed using two different anti-lamin B2 antibodies and lamin B2 knockdown. The discrepancy might be explained by differences in cell lines or techniques of immunofluorescence.

This study further showed the co-localization of mitotic lamin B2 with an inner nuclear membrane protein SUN1 outside the spindle poles (Figure 6f). SUN1 is known to interact with outer nuclear membrane protein nesprins.[29,34] SUN1 and nesprins bind to lamins and cytoskeletal components, respectively, resulting in nuclear-cytoplasmic connection in interphase cells.[32] In addition, SUN1 was reported to mediate attachment of the nucleus to the centrosome in *C. elegans*.[31] These results indicate that the lamin–SUN1–nesprin complex stabilizes the position of the nucleus in a cell. Intriguingly, nesprin-2 and nesprin-3 were also identified by LC-MS/MS from lamin B2 immunoprecipitates prepared from mitotic HCT116 cells (Supplementary Table S1), suggesting that mitotic lamin B2 makes a complex with SUN1 and nesprins outside the spindle poles. Although the effect of the non-mitotic function of lamin B2 in mitotic processes is unknown, these results imply that the lamin B2 mitotic structure contributes to stabilization of the spindle poles and mitotic spindles.

As CIN is involved in tumorigenesis and tumor progression, prevention of CIN might be an approach for cancer therapy. A number of reports have shown that aberrant expression of mitotic proteins induces chromosome mis-segregation and causes CIN; however, it is unknown whether most of these proteins actively prevent mitotic defects. Recently, two microtubule-depolymerizing kinesins, Kif2b and MCAK, have been shown to actively prevent chromosome mis-segregation in CIN cancer cell lines.[35] Ectopic expression of these kinesins corrects improper microtubule attachment to kinetochores, leading to protection from chromosome mis-segregation. Our data showed that ectopic expression of lamin B2 in CIN cancer cells rescues aneuploidy and mitotic defects such as chromosome mis-segregation, mitotic delay and aberrant spindle formation (Figures 4 and 5), suggesting that forced expression of lamin B2 seems to promote the correction of chromosome segregation. Given that lamin B2 expression levels are enhanced in HNPCC MIN-type cancer as compared with not only CIN-type cancer but also non-tumor epithelium (Figure 7), enhanced lamin B2 expression in MIN cancer cells might be actively preventing CIN.

Our results may contribute to develop a novel strategy for cancer therapy that specifically targets aneuploid cancer cells. A recent report showed that proliferation of aneuploid, but not euploid, cancer cells is inhibited by AICAR, 17-AAG, chloroquine or their combination.[36] On the other hand, recent meta-analysis identified that MIN tumor patients do not benefit from fluorouracil-based adjuvant chemotherapy.[37] In this respect, determination of the state of chromosome stability of cancer may support a strategy for cancer therapy. Further study is needed to evaluate whether CIN-causative protein lamin B2 is a useful marker for planning a cancer therapy strategy as well as whether ectopic expression of lamin B2 is useful for CIN-preventing therapy.

MATERIALS AND METHODS

Cell culture and cell-cycle synchronization

Caco-2, HCT116, SW48, WiDr and RKO colorectal cancer cell lines were purchased from ATCC (Manassas, VA, USA). HT29 and SW480 cell lines and DLD1 and SW837 cell lines were kindly provided by Dr Takenaga and Dr Tagawa (Chiba Cancer Center Research Institute, Chiba, Japan), respectively. Cells were grown at 37 °C in 5% CO_2 in IMDM or RPMI-1640 (Invitrogen, Carlsbad, CA, USA) supplemented with 10% fetal bovine serum (Invitrogen) and 1% penicillin-streptomycin (Invitrogen). To accumulate mitotic cells, cells were pre-synchronized at the G_1/S phase upon treatment with 2 mM thymidine for 16 h and then released into fresh medium for 10–12 h.

Plasmid DNA, siRNA and antibodies

To generate lamin B2-GFP and lamin B2-mCherry plasmids, cDNA encoding human lamin B2 was amplified from HeLa cells by PCR using the forward primer 5′-TAAAGCTTATATGGCCACGCCGCTGCCC-3′ and the reverse primer 5′-ATAGGTACCCACATCACGTAGCAGCCTCTT-3′, and was cloned into pEGFP-N1 or pmCherry-N1 vector plasmids (Clontech, Palo Alto, CA, USA). To generate the mCherry-α-tubulin plasmid, full-length human α-tubulin cDNA was amplified from HeLa cells by PCR using the forward primer 5′-GCAAAGATCTATGCGTGAGTGCATCTCCATCC-3′ and the reverse primer 5′-GCGGGGATCCTTAGTATTCCTCTCCTTCTTC-3′, and was cloned into the pmCherry-C1 vector plasmid (Clontech). The histone H2B-GFP plasmid[38] was kindly provided by Dr Kimura (Kyoto University, Kyoto, Japan). Plasmids encoding lamin B2-shRNA (TRCN0000255440, TRCN0000255441, TRCN0000255443 and TRCN0000255444) or non-target control shRNA (SHC216) were purchased from Sigma-Aldrich (St Louis, MO, USA). Lamin B2-siRNA duplex (TCGGCAATAGCTCACCGTTTA) was purchased from Qiagen (Hilden, Germany) and Invitrogen (LMNB2-HSS189214). siRNA duplexes targeting lamins A/C (LMNA-HSS106094) and B1 (LMNB1-HSS106096) were purchased from Invitrogen. siRNA targeting SUN1 (Hs_UNC84A_2809) was purchased from Sigma-Aldrich. Control siRNAs were purchased from Qiagen (Firefly luciferase GL2-siRNA) and Invitrogen (Medium GC Duplex#2). Antibodies to the following proteins were purchased: mouse (LN43; Abcam, Cambridge, UK) and rabbit (Proteintech Group, Chicago, IL, USA) anti-lamin B2, goat anti-lamin B1 (sc-6216; Santa Cruz Biotechnology, Santa Cruz, CA, USA), mouse anti-lamin A/C (636; Santa Cruz Biotechnology), mouse (DM1A; Sigma-Aldrich) and rat (YOL1/34; Santa Cruz Biotechnology) anti-α-tubulin, mouse anti-β-tubulin

(TUB2.1; Sigma-Aldrich), mouse anti-GFP (Roche, Basel, Switzerland), rabbit anti-DsRed (Clontech), rabbit anti-KIF11 (Eg5) (HPA010568; Sigma-Aldrich), rabbit anti-SUN1 (sc-135077; Santa Cruz Biotechnology), and goat anti-actin (C-11; Santa Cruz Biotechnology) antibodies. Alexa Fluor 488 goat anti-mouse IgG and Alexa Fluor 594 goat anti-mouse IgG antibodies were purchased from Molecular Probes (Eugene, OR, USA). HRP-conjugated anti-mouse IgG (Dako, Glostrup, Denmark), anti-rabbit IgG (GE Healthcare, Little Chalfont, UK) and anti-goat IgG (MP Biomedicals, Santa Ana, CA, USA) antibodies were used.

Protein extraction and western blotting

Nuclear extracts were obtained from $\sim 1 \times 10^8$ cells. Cells were resuspended in 5 ml cold buffer (20 mM HEPES-KOH (pH 7.4), 20 mM KCl, 1 mM DTT, 0.1% NP-40, and Complete protease inhibitor cocktail; Roche) and allowed to swell on ice for 15 min. Then, cells were homogenized with a Dounce homogenizer or vigorously vortexed for 15 s 2 times and centrifuged for 5 min at 1000 r.p.m. After pellets were washed twice with the same cold buffer, they were solubilized in lysis buffer (7 M urea, 2 M thiourea, 4% w/v CHAPS, 30 mM Tris–HCl (pH 8.5) and Complete) by passing through 26-gauge needles and were then ultracentrifuged for 1 h at 100 000 *g*. For extraction of whole-cell proteins, cells were directly lysed in SDS–PAGE sample buffer. Western blotting was performed using the enhanced chemiluminescence (ECL) detection system (GE Healthcare), as described previously.[22,39]

RT–PCR

Extraction of total RNA and cDNA synthesis were performed as described previously.[40] The expression levels of lamin B2 mRNA were examined by PCR using the forward primer 5′-TCCGCACCGTCCTGGTTA-3′ and the reverse primer 5′-CCTGTTGGTGGAAAAGATCCTC-3′. The primer pair for GAPDH (RPP-401) was purchased from TOYOBO (Osaka, Japan).

Agarose 2D-DIGE and protein identification

Agarose 2D-DIGE was performed as described previously.[41] Pooled nuclear extracts (50 μg) of CIN cell lines (HT29, SW480, SW837 and Caco-2) and MIN cell lines (HCT116, RKO, DLD1 and SW48) were labeled with 400 pmol of Cy5 and Cy3, respectively. Internal standard, created by pooling aliquots of all the samples, was labeled with Cy2. The mixed labeled extract (50 μg each) was applied to agarose 2D-DIGE. In-gel tryptic digestion of proteins and identification by mass spectrometry were performed as described previously.[41,42]

Immunoprecipitation-LC-MS/MS

To collect mitotic HCT116 cells, cells were treated with 10 μM RO-3306 (Enzo Life Sciences, Farmingdale, NY, USA) for 19 h to arrest the cell cycle at G_2 phase and then cultured in fresh medium without the drug for further 45 min. To prepare cell lysates used for immunoprecipitation (IP lysates), cells were suspended in phosphate-buffered saline containing 1% NP-40, Complete, and phosphatase inhibitor cocktail PhosSTOP (Roche), and then homogenized by sonication. After centrifugation at 100 000 *g* for 30 min, the supernatant was collected. Immunoprecipitation was performed using anti-lamin B2 (LN43), A/C, or B1 antibody crosslinked to Protein G Dynabeads (Invitrogen) using dimethyl pimelimidate. IP lysates were reacted with antibody-coated Dynabeads for 1 h at 4 °C, and the absorbed proteins were eluted with SDS–PAGE sample buffer free of reducing agents. After reduction with β-mercaptoethanol, immunoprecipitates were resolved by SDS–PAGE and the gel lane was divided into several pieces, and in-gel tryptic digestion of proteins was performed as described previously.[43] The digested peptides were analyzed by LTQ-Orbitrap XL.[44] Protein identification was performed using the MASCOT search engine v2.4 (the UniProtKB/Swiss-Prot database 2012_6). Database search parameters were the charge of the precursor ion, 2+ and 3+; peptide mass tolerance, 3 p.p.m.; fragment tolerance, 0.6 Da; allowing up to one missed cleavage; fixed modification, carbamidomethylation of cysteine; variable modification, oxidation of methionine. Proteins were identified based on at least two unique peptides. The number of assigned spectra was calculated by the Scaffold 3 software (Proteome Software, Portland, OR, USA) for semiquantitation.

Immunostaining and FISH of cell lines

For immunostaining, cells were fixed with acetone for 10 min at 4 °C (Figures 1c and 3) or 4% HCHO for 20 min at room temperature (Figures 4d and e) or 30 °C (Figure 6), and HCHO-fixed cells were permeabilized in phosphate-buffered saline containing 0.5% Triton X-100 on ice. After blocking in phosphate-buffered saline containing 3% bovine serum albumin and 0.1% Tween-20, cells were stained with appropriate antibodies. Immunostained cells were viewed under an LSM710 confocal microscope with the Zen software (Carl Zeiss, Jena, Germany). The objective lenses were EC Plan-NEO FLUAR × 40/1.3 and Plan APOCHROMAT × 63/1.4. FISH was performed as described previously.[9,10] Probes to the pericentromeric regions of chromosome 7, 8, 12 and 15 were purchased from Vysis (Downers Grove, IL, USA). FISH-stained cells were viewed under a Zeiss fluorescent microscope with a × 40/1.3 or a × 63/1.4 oil immersion objective and an AxioVision digital imaging system (Carl Zeiss).

Transient and stable transfection

Transfection with plasmids or siRNA was performed using Lipofectamine 2000 or RNAiMAX (Invitrogen) as described previously.[9,10] For stable transfection, HCT116 or WiDr cells were transfected with histone H2B-GFP, mCherry-α-tubulin, lamin B2-shRNA, or control shRNA expression plasmid containing the neomycin- or puromycin-resistant gene and then selected in medium containing 400 μg/ml geneticin (Invitrogen) or 4 μg/ml puromycin (StressMarq Biosciences, Victoria, BC, Canada).

Live-cell imaging

Cells expressing histone H2B-GFP or mCherry-α-tubulin were mounted on a Zeiss LSM510 confocal microscope equipped with a heating stage (37 °C), CO_2 (5%) incubation chamber, and a × 40/1.2 water immersion or a × 63/1.4 oil immersion objective (Carl Zeiss). Cells were monitered at 3- or 5-min intervals. To detect the total fluorescence of histone H2B-GFP or mCherry-α-tubulin in a cell, z-stack images from the cell bottom to the cell top were collected and merged into a single plane at each time point during time-lapse experiments.

Patients and immunohistochemistry

From HNPCC and sporadic colorectal cancer patients, paraffin-embedded blocks of tumor tissues were collected in the Department of Frontier Surgery, Chiba University Hospital. The definition of HNPCC is based on the Amsterdam II criteria.[33,45] The ethics committee of the Graduate School of Medicine, Chiba University approved the protocol. Written informed consent was obtained from each patient before surgery. Four-micrometer sections from paraffin tissues were fixed on slide glasses. Tissues were immunostained as described previously.[46] After deparaffinization and antigen retrieval with microwave irradiation for 5 min in pH 6.0 citric buffer three times, tissues were stained using anti-lamin B2 antibody and En Vision + (Dako). Tissue sections were counterstained with hematoxylin. Using the TissueFAXS system and the corresponding HistoQuest software, stained tissues were viewed and lamin B2 staining was quantitated. Normal epithelial and cancer cells in at least 12 areas in each tissue section were analyzed for the mean intensity of lamin B2 staining, and the average value was calculated.

CONFLICT OF INTEREST

The authors declare no conflict of interest.

ACKNOWLEDGEMENTS

We would like to thank Hironori Funabiki for critical reading of this manuscript and Masumi Ishibashi for technical assistance. This work was supported by a Grant-in-Aid for Research on Biological Markers for New Drug Development H20-0005 to TT from the Ministry of Health, Labour and Welfare of Japan and by a Grant-in-Aid 21390354 to TT from the Ministry of Education, Science, Sports and Culture of Japan. This work was supported by a Grant-in-Aid for Research on Biological Markers for New Drug Development H20-0005 to TT from the Ministry of Health, Labour and Welfare of Japan and by a Grant-in-Aid 21390354 to TT from the Ministry of Education, Science, Sports and Culture of Japan.

REFERENCES

1 Lengauer C, Kinzler KW, Vogelstein B. Genetic instability in colorectal cancers. *Nature* 1997; **386**: 623–627.
2 Lengauer C, Kinzler KW, Vogelstein B. Genetic instabilities in human cancers. *Nature* 1998; **396**: 643–649.

3 Rajagopalan H, Lengauer C. Aneuploidy and cancer. *Nature* 2004; **432**: 338–341.
4 Holland AJ, Cleveland DW. Boveri revisited: chromosomal instability, aneuploidy and tumorigenesis. *Nat Rev Mol Cell Biol* 2009; **10**: 478–487.
5 Bischoff JR, Anderson L, Zhu Y, Mossie K, Ng L, Souza B *et al.* A homologue of Drosophila aurora kinase is oncogenic and amplified in human colorectal cancers. *EMBO J* 1998; **17**: 3052–3065.
6 Kops GJ, Weaver BA, Cleveland DW. On the road to cancer: aneuploidy and the mitotic checkpoint. *Nat Rev Cancer* 2005; **5**: 773–785.
7 Yuen KW, Montpetit B, Hieter P. The kinetochore and cancer: what's the connection? *Curr Opin Cell Biol* 2005; **17**: 576–582.
8 Zhou H, Kuang J, Zhong L, Kuo WL, Gray JW, Sahin A *et al.* Tumour amplified kinase STK15/BTAK induces centrosome amplification, aneuploidy and transformation. *Nat Genet* 1998; **20**: 189–193.
9 Tomonaga T, Matsushita K, Yamaguchi S, Oohashi T, Shimada H, Ochiai T *et al.* Overexpression and mistargeting of centromere protein-A in human primary colorectal cancer. *Cancer Res* 2003; **63**: 3511–3516.
10 Tomonaga T, Matsushita K, Ishibashi M, Nezu M, Shimada H, Ochiai T *et al.* Centromere protein H is up-regulated in primary human colorectal cancer and its overexpression induces aneuploidy. *Cancer Res* 2005; **65**: 4683–4689.
11 Tomonaga T, Nomura F. Chromosome instability and kinetochore dysfunction. *Histol Histopathol* 2007; **22**: 191–197.
12 Fawcett DW. On the occurrence of a fibrous lamina on the inner aspect of the nuclear envelope in certain cells of vertebrates. *Am J Anat* 1966; **119**: 129–145.
13 Liu J, Rolef Ben-Shahar T, Riemer D, Treinin M, Spann P, Weber K *et al.* Essential roles for Caenorhabditis elegans lamin gene in nuclear organization, cell cycle progression, and spatial organization of nuclear pore complexes. *Mol Biol Cell* 2000; **11**: 3937–3947.
14 Ma L, Tsai M-Y, Wang S, Lu B, Chen R, Yates III JR *et al.* Requirement for Nudel and dynein for assembly of the lamin B spindle matrix. *Nat Cell Biol* 2009; **11**: 247–256.
15 Maeshima K, Yahata K, Sasaki Y, Nakatomi R, Tachibana T, Hashikawa T *et al.* Cell-cycle-dependent dynamics of nuclear pores: pore-free islands and lamins. *J Cell Sci* 2006; **119**: 4442–4451.
16 Shaklai S, Amariglio N, Rechavi G, Simon AJ. Gene silencing at the nuclear periphery. *FEBS J* 2007; **274**: 1383–1392.
17 Shimi T, Pfleghaar K, Kojima S, Pack CG, Solovei I, Goldman AE *et al.* The A- and B-type nuclear lamin networks: microdomains involved in chromatin organization and transcription. *Genes Dev* 2008; **22**: 3409–3421.
18 Spann TP, Moir RD, Goldman AE, Stick R, Goldman RD. Disruption of nuclear lamin organization alters the distribution of replication factors and inhibits DNA synthesis. *J Cell Biol* 1997; **136**: 1201–1212.
19 Spann TP, Goldman AE, Wang C, Huang S, Goldman RD. Alteration of nuclear lamin organization inhibits RNA polymerase II-dependent transcription. *J Cell Biol* 2002; **156**: 603–608.
20 Stewart CL, Roux KJ, Burke B. Blurring the boundary: the nuclear envelope extends its reach. *Science* 2007; **318**: 1408–1412.
21 Tsai M-Y, Wang S, Heidinger JM, Shumaker DK, Adam SA, Goldman RD *et al.* A mitotic lamin B matrix induced by RanGTP required for spindle assembly. *Science* 2006; **311**: 1887–1893.
22 Kuga T, Nozaki N, Matsushita K, Nomura F, Tomonaga T. Phosphorylation statuses at different residues of lamin B2, B1, and A/C dynamically and independently change throughout the cell cycle. *Exp Cell Res* 2010; **316**: 2301–2312.
23 Maeshima K, Iino H, Hihara S, Funakoshi T, Watanabe A, Nishimura M *et al.* Nuclear pore formation but not nuclear growth is governed by cyclin-dependent kinases (Cdks) during interphase. *Nat Struct Mol Biol* 2010; **17**: 1065–1071.
24 Dechat T, Pfleghaar K, Sengupta K, Shimi T, Shumaker DK, Solimando L *et al.* Nuclear lamins: major factors in the structural organization and function of the nucleus and chromatin. *Genes Dev* 2008; **22**: 832–853.
25 Georgatos SD, Pyrpasopoulou A, Theodoropoulos PA. Nuclear envelope breakdown in mammalian cells involves stepwise lamina disassembly and microtubule-drive deformation of the nuclear membrane. *J Cell Sci* 1997; **110**: 2129–2140.
26 Maison C, Pyrpasopoulou A, Theodoropoulos PA, Georgatos SD. The inner nuclear membrane protein LAP1 forms a native complex with B-type lamins and partitions with spindle-associated mitotic vesicles. *EMBO J* 1997; **16**: 4839–4850.
27 Tsushimi T, Noshima S, Oga A, Esato K, Sasaki K. DNA amplification and chromosomal translocations are accompanied by chromosomal instability: analysis of seven human colon cancer cell lines by comparative genomic hybridization and spectral karyotyping. *Cancer Genet Cytogenet* 2001; **126**: 34–38.
28 Thompson SL, Compton DA. Examining the link between chromosomal instability and aneuploidy in human cells. *J Cell Biol* 2008; **180**: 665–672.
29 Crisp M, Liu Q, Roux K, Rattner JB, Shanahan C, Burke B *et al.* Coupling of the nucleus and cytoplasm: role of the LINC complex. *J Cell Biol* 2006; **172**: 41–53.
30 Haque F, Lloyd DJ, Smallwood DT, Dent CL, Shanahan CM, Fry AM *et al.* SUN1 interacts with nuclear lamin A and cytoplasmic nesprins to provide a physical connection between the nuclear lamina and the cytoskeleton. *Mol Cell Biol* 2006; **26**: 3738–3751.
31 Malone CJ, Misner L, Le Bot N, Tsai MC, Campbell JM, Ahringer J *et al.* The C. elegans hook protein, ZYG-12, mediates the essential attachment between the centrosome and nucleus. *Cell* 2003; **115**: 825–836.
32 Razafsky D, Hodzic D. Bringing KASH under the SUN: the many faces of nucleo-cytoskeletal connections. *J Cell Biol* 2009; **186**: 461–472.
33 Lynch HT, de la Chapelle A. Hereditary colorectal cancer. *New Engl J Med* 2003; **348**: 919–932.
34 Stewart-Hutchinson PJ, Hale CM, Wirtz D, Hodzic D. Structural requirements for the assembly of LINC complexes and their function in cellular mechanical stiffness. *Exp Cell Res* 2008; **314**: 1892–1905.
35 Bakhoum SF, Thompson SL, Manning AL, Compton DA. Genome stability is ensured by temporal control of kinetochore-microtubule dynamics. *Nat Cell Biol* 2009; **11**: 27–35.
36 Tang YC, Williams BR, Siegel JJ, Amon A. Identification of aneuploidy-selective antiproliferation compounds. *Cell* 2011; **144**: 499–512.
37 Des Guetz G, Schischmanoff O, Nicolas P, Perret GY, Morere JF, Uzzan B. Does microsatellite instability predict the efficacy of adjuvant chemotherapy in colorectal cancer? A systematic review with meta-analysis. *Eur J Cancer* 2009; **45**: 1890–1896.
38 Kanda T, Sullivan KF, Wahl GM. Histone-GFP fusion protein enables sensitive analysis of chromosome dynamics in living mammalian cells. *Curr Biol* 1998; **8**: 377–385.
39 Kuga T, Hoshino M, Nakayama Y, Kasahara K, Ikeda K, Obata Y *et al.* Role of Src-family kinases in formation of the cortical actin cap at the dorsal cell surface. *Exp Cell Res* 2008; **314**: 2040–2054.
40 Kuga T, Kume H, Kawasaki N, Sato M, Adachi J, Shiromizu T *et al.* A novel mechanism of keratin cytoskeleton organization through casein kinase Iα and FAM83H in colorectal cancer. *J Cell Sci* 2013; **126**: 4721–4731.
41 Nishimori T, Tomonaga T, Matsushita K, Oh-Ishi M, Kodera Y, Maeda T *et al.* Proteomic analysis of primary esophageal squamous cell carcinoma reveals downregulation of a cell adhesion protein, periplakin. *Proteomics* 2006; **6**: 1011–1018.
42 Tomonaga T, Matsushita K, Yamaguchi S, Oh-Ishi M, Kodera Y, Maeda T *et al.* Identification of altered protein expression and post-translational modifications in primary colorectal cancer by using agarose two-dimensional gel electrophoresis. *Clin Cancer Res* 2004; **10**: 2007–2014.
43 Adachi J, Kumar C, Zhang Y, Mann M. In-depth analysis of the adipocyte proteome by mass spectrometry and bioinformatics. *Mol Cell Proteomics* 2007; **6**: 1257–1273.
44 Narumi R, Murakami T, Kuga T, Adachi J, Shiromizu T, Muraoka S *et al.* A strategy for large-scale phosphoproteomics and SRM-based validation of human breast cancer tissue samples. *J Proteome Res* 2012; **11**: 5311–5322.
45 Vasen HF, Watson P, Mecklin JP, Lynch HT. New clinical criteria for hereditary nonpolyposis colorectal cancer (HNPCC, Lynch syndrome) proposed by the International Collaborative group on HNPCC. *Gastroenterology* 1999; **116**: 1453–1456.
46 Seimiya M, Tomonaga T, Matsushita K., Sunaga M, Oh-Ishi M, Kodera Y *et al.* Identification of novel immunohistochemical tumor markers for primary hepatocellular carcinoma; clathrin heavy chain and formiminotransferase cyclodeaminase. *Hepatology* 2008; **48**: 519–530.

Supplementary Information accompanies this paper on the Oncogenesis website (http://www.nature.com/oncsis)

Clinicopathological Significance of Leucine-Rich α2-Glycoprotein-1 in Sera of Patients With Pancreatic Cancer

AQ1 *Kenta Furukawa, MD,* Koichi Kawamoto, MD, PhD,* Hidetoshi Eguchi, MD, PhD,* Masahiro Tanemura, MD, PhD,† Tsukasa Tanida, MD,* Yoshito Tomimaru, MD, PhD,* Hirofumi Akita, MD, PhD,* Naoki Hama, MD, PhD,* Hiroshi Wada, MD, PhD,* Shogo Kobayashi, MD, PhD,* Yuji Nonaka, MS,‡ Shinji Takamatsu, PhD,‡ Shinichiro Shinzaki, MD, PhD,‡ Takashi Kumada, MD, PhD,§ Shinji Satomura, PhD,‖ Toshifumi Ito, MD, PhD,¶ Satoshi Serada, PhD,# Tetsuji Naka, MD, PhD,# Masaki Mori, MD, PhD,* Yuichiro Doki, MD, PhD,* Eiji Miyoshi, MD, PhD,‡ and Hiroaki Nagano, MD, PhD**

Objectives: Leucine-rich α2-glycoprotein-1 (LRG-1) is an inflammatory protein. Serum LRG-1 levels can reportedly be used as a cancer biomarker for several types of carcinoma. In the present study, we investigated the clinical usefulness of serum LRG-1 levels as a biomarker of pancreatic cancer.

Methods: A total of 124 patients with pancreatic cancer, 35 patients with chronic pancreatitis (CP), and 144 healthy volunteers were enrolled in the study. Serum LRG-1 levels were assayed by enzyme-linked immunosorbent assay. Immunohistochemistry was used to examine LRG-1 expression in pancreatic cancer tissues.

Results: Serum LRG-1 levels were significantly increased in patients with pancreatic cancer compared with CP patients and healthy volunteers. The LRG-1 levels increased with progressive clinical stages of pancreatic cancer. Receiver operator curve analysis showed that a combination of carbohydrate antigen 19-9 and LRG-1 resulted in a higher area under the curve for the diagnosis of pancreatic cancer. Positive staining was observed in all cases of pancreatic cancer, but positive signal was scarcely detected in tissues from CP patients or normal surrounding tissue.

Conclusions: These results suggest that serum LRG-1 is a promising biomarker for pancreatic cancer.

Key Words: leucine-rich α2-glycoprotein-1, pancreatic cancer, biomarker

(*Pancreas* 2014;00: 00–00)

Pancreatic cancer is the fourth leading cause of cancer-related death in the United States.[1] Pancreatic ductal adenocarcinoma (PDAC) is the most common form of pancreatic cancer. In Japan, the mortality rate for PDAC has increased over the past decade, currently ranking fifth.[2] Pancreatic ductal adenocarcinoma has an extremely poor prognosis with a 5-year survival rate of less than 5%. Early detection of PDAC remains clinically challenging because of its asymptomatic nature, and surgery offers the only potential cure. However, the 5-year survival of PDAC patients after curative resection (surgery alone) is estimated to be 10% to 20%.[3] Curative surgery with adjuvant chemotherapy improves overall survival,[4] but the clinical outcome of pancreatic cancer has not been markedly improved. One strategy that could improve PDAC survival is to detect the cancer in its early clinical stages. Thus, there is an urgent need to develop biomarkers for the stratification of patients for current treatment modalities and the development of novel therapeutic strategies.

Molecules that are specifically overexpressed in tumors not only serve as useful diagnostic markers, but also as potential therapeutic targets.[5] The development of methods that are sensitive and specific enough to permit an early diagnosis of PDAC may facilitate the detection and subsequent treatment of this disease. However, an important factor adds another level of complexity to this already demanding task. A number of overlapping symptomatological features are known to link pancreatic adenocarcinoma to the inflammatory disease chronic pancreatitis (CP), often obscuring the distinction between these 2 pathological conditions.

Carcinoembryonic antigen, carbohydrate antigen 19-9 (CA19-9), and DUPAN-2 are the only serum biomarkers currently available for AQ3 PDAC detection and have shown some utility as diagnostic adjuncts and prognostic markers in Japan.[6] However, these markers are not widely used in routine clinical practice in Europe and America due to low sensitivity, specificity, or reproducibility and therefore cannot be routinely used to diagnose PDAC. Although CA19-9 is not a specific marker, identifying characteristic CA19-9 carrier proteins may allow higher specificity (molecular proteomics). Although the detection of CA19-9 carrier proteins is established, it will be very difficult to detect the early stage of pancreatic cancer.[7] To establish a next-generation biomarker for pancreatic cancer, combination assays of several cancer biomarkers or a novel type of cancer biomarker involved in CP will be required.

Leucine-rich α2-glycoprotein-1 (LRG-1) was first identified in 1977 as an inflammatory protein in human serum.[8] Recent studies have demonstrated that serum LRG-1 can be used as a biomarker in several kinds of cancer, including ovarian, lung, biliary tract, and hepatocellular carcinoma related to hepatitis B virus infection.[9–13] Increased serum LRG-1 levels in patients with pancreatic cancer were first reported using multidimensional liquid chromatography followed by 2-dimensional difference gel electrophoresis in plasma proteomics.[14] The authors used Western blot to confirm the increase in serum LRG-1 patients with pancreatic cancer compared with healthy volunteers (HVs), and they showed that patients with CP tended to express lower serum levels of LRG-1 than patients with PDAC. However, they did not find significant differences between patients with CP and patients with PDAC due, at least in part, to the limited number of patients in the study. The study did not investigate the relationships between the marker and the clinical stages of pancreatic cancer, and no immunological study of LRG-1 in pancreatic cancer was performed. As LRG-1 has also been reported to be part of an acute inflammatory

AQ2 From the *Department of Surgery, Osaka University Graduate School of Medicine, Osaka; †Department of Surgery and Institute for Clinical Research National Hospital Organization Kure Medical Center and Chugoku Cancer Center, Hiroshima; ‡Department of Molecular Biochemistry and Clinical Investigation, Osaka University Graduate School of Medicine, Osaka; §Department of Gastroenterology, Ogaki Municipal Hospital, Ogaki; ‖Wako Pure Chemical Industries, Ltd; ¶Department of Gastroenterology and Hepatology, Japan Community Health Care Organization Osaka Hospital; and #Laboratory for Immune Signal, National Institute of Biomedical Innovation, Osaka, Japan.

Received for publication November 25, 2013; accepted June 20, 2014.

Reprints: Hiroaki Nagano, MD, PhD, Department of Surgery, Osaka University, Graduate School of Medicine, Suita, Yamadaoka 2-2, Osaka 565-0871, Japan (e-mail: hnagano@gesurg.med.osaka-u.ac.jp).

The authors declare no conflict of interest.

response in ulcerative colitis and acute appendicitis, LRG-1 may be increased as a result of inflammation.[15–18]

In the present study, we determined serum LRG-1 levels in patients with CP and PDAC and assessed the clinicopathological significance of the increase in LRG-1 in terms of clinical parameters and immunohistochemistry.

MATERIALS AND METHODS

Patients and Sample Collection

Peripheral blood samples from patients with pancreatic disease and apparently HVs were obtained from Ogaki Municipal Hospital, Japan Community Health Care Organization Osaka Hospital, and Osaka University Hospital. Written informed consent was obtained from all patients and HVs. The study was performed in accordance with the guidelines issued by the local institutional review board of Osaka University. Sera from 124 patients with PDAC and 35 patients with CP were evaluated. All blood sampling was done at the time of diagnosis (pretreatment). A total of 144 serum samples from HVs were used as controls. Detailed information on clinical background was available for 71 PDAC patients, 20 CP patients, and 91 HVs. The collection, processing, and storage of all blood samples were standardized as follows: blood samples were collected in a vacutainer tube, allowed to clot at room temperature for 30 minutes, and then centrifuged at ~2500 × g for 10 minutes. The serum was removed and immediately divided into 100-μL and 1-mL aliquots and stored at −80°C until use.

Formalin-fixed, paraffin-embedded tissue blocks from patients with PDAC were obtained from surgical cases at Osaka University Hospital in 2011 and 2012. Eleven PDAC, 1 CP, and 3 noncystic lesions of intraductal papillary mucinous neoplasm (IPMN; control for normal pancreas) were randomly selected.

Quantification of Serum LRG-1

Serum LRG-1 levels were determined using the human LRG assay kit (IBL, Fujioka, Japan) according to the manufacturer's protocol. Briefly, each serum sample was diluted (1:100) with buffer from the kit and the assays performed in triplicate. The LRG-1 levels were determined from a standard curve created using control samples. If the concentration of serum LRG-1 was less than 1.56 ng/mL or greater than 100 ng/mL, the dilution rate was changed.

Serum CA19-9 levels were measured in the hospital laboratory at the time of diagnosis.

Statistical Analysis

All statistical analyses were performed using JMP (version 9.0; SAS Institute Inc, Japan). Continuous data between clinical groups were compared by the Mann-Whitney *U* test for nonparametric data and the Student *t* test for normally distributed data. The Pearson product–moment correlation coefficient was used to examine associations between 2 continuous variables. Associations between categorical variables were examined using Fisher exact test. Normal cutoffs were defined for LRG-1 as the optimum point at which sensitivity and specificity was maximized. Receiver operating characteristic (ROC) curves were generated, and the areas under the curve (AUCs) were defined.

Immunohistochemical Staining

To analyze LRG-1 expression by immunohistochemistry, formalin-fixed, paraffin-embedded tissue blocks from patients with pancreatic cancer were deparaffinized in xylene and rinsed in a series of 100%, 95%, 90%, 80%, 70%, and 60% ethanol solutions. The antigen was recovered by incubating the slides in 10 mmol/L citrate buffer (pH 6.0) for 40 minutes in boiling water. To quench endogenous peroxidase activity, the slides were incubated with 0.3% H_2O_2 in methanol for 30 minutes and then rinsed extensively in phosphate-buffered saline. The slides were incubated with blocking serum for 20 minutes followed by a 1:400 dilution of rabbit anti-LRG monoclonal antibody (Cat# 13224-1-AP; ProteinTech Group, Chicago, Ill) overnight at 4°C. Endogenous biotin activity was blocked using an avidin D–biotin blocking solution before in situ localization of the antigen using a biotin-avidin antigen detection method (R.T.U. Vectastain kit, Vector Laboratories, Burlingame, Calif). After extensive washing in phosphate-buffered saline, sections were incubated in a diaminobenzidine solution (Stable DAB, Invitrogen, Carlsbad, Calif) and counterstained with a hematoxylin solution. The slides were then dehydrated by washing in ethanol and cleared in xylene. Cover slips were placed on the slides, which were evaluated for LRG-1 staining. The intensity of LRG-1 staining was scored on a scale of 0 to 2 (0, no staining; 1, moderate staining; 2, strong staining).

RESULTS

Quantification of Serum LRG-1 Levels

Serum LRG-1 levels were significantly elevated in patients with PDAC (7.99 [5.07] μg/mL) compared with HVs (3.51 [1.42] μg/mL) and patients with CP (4.96 [2.11] μg/mL) ($P < 0.001$; Fig. 1, Table 1). F1 T1

When 71 patients with pancreatic cancer were investigated in terms of clinical stage, the mean (SD) LRG-1 concentrations significantly increased with the progression of clinical stage as follows: 3.33 (0.66) μg/mL in stage I, 7.07 (4.18) μg/mL in stage II, 8.74 (5.86) μg/mL in stage III, and 8.72 (4.35) μg/mL in stage IV (Fig. 2). Among them, significant difference of the LRG-1 concentrations was observed between stage I and the other stages, but the differences between stage II and III, III and IV, and II and IV were not significant. The mean (SD) LRG-1 concentration was F2

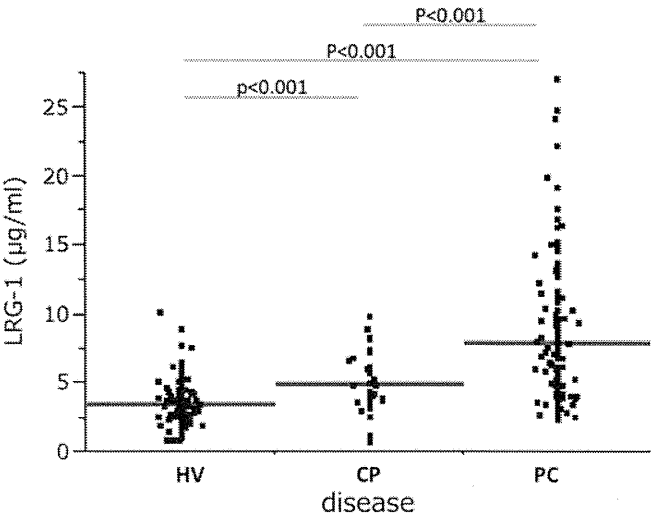

FIGURE 1. Detection of serum LRG-1 by enzyme-linked immunosorbent assay. Serum LRG-1 concentrations were determined for 124 patients with PDAC, 35 patients with CP, and 144 HVs. The mean (SD) LRG-1 concentration for PDAC patient sera was 7.99 (5.07) μg/mL compared with 3.51 (1.42) μg/mL for HV sera ($P < 0.001$) and 4.96 (2.11) μg/mL for CP patients ($P < 0.001$).

TABLE 1. Clinicopathological Characteristics of Patients With PDAC, HVs, and Patients With CP

	PDAC (n = 124)	HV (n = 144)	CP (n = 35)	PDAC vs HV	PDAC vs CP
Age, y*	66.4 (7.83)	44.9 (12.5)	66.7 (10.6)	$P < 0.01$	NS
Sex, % male	70.4	59.3	60.0	NS	NS
LRG-1, μg/mL*	7.99 (5.07)	3.51 (1.42)	4.96 (2.11)	$P < 0.01$	$P < 0.01$
CA19-9, U/mL*	213.7 (208.1)	13.3 (9.61)	7.88 (8.88)	$P < 0.01$	$P < 0.01$
Tumor location (head/body, tail)	42/29				
Lymph node metastasis (positive/negative)	31/40				
Clinical stage (1/2/3/4)†	6/28/21/16				

*Data are presented as mean (SD).

AQ5 †General Rules for the Study of Pancreatic Cancer, 6th edition (Japan Pancreas Society).

NS indicates not significant.

significantly higher in the lymph node metastasis–positive group than AQ6 the lymph node metastasis–negative group (9.23 [4.68] μg/mL and 6.51 [4.69] μg/mL, respectively; $P < 0.001$). These results clearly demonstrate that in patients with PDAC, LRG-1 can be associated with local progression or lymph node metastasis of the primary tumor, but not with distant progression, such as liver metastasis. In addition, serum LRG-1 levels positively correlated with CA19-9 ($R^2 = 0.088$, $P < 0.001$), but not with carcinoembryonic antigen ($R^2 = 0.017$, $P = 0.27$).

ROC Curve Analysis and Diagnostic Performance

The ROC curve analysis was performed to determine the clinical usefulness of LRG-1 for diagnosing pancreatic cancer. F3 As shown in Figure 3A, CA19-9 was useful for differentiating patients with PDAC from HVs with AUC of 0.869. At a cutoff value of 37 U/mL for CA19-9, the optimal sensitivity and specificity were 71.9% and 96.4%, respectively. Similar analysis indicated that the AUC for LRG-1 was 0.850. At a cutoff value of 4.81 μg/mL for LRG-1, the optimal sensitivity and specificity were 67.7% and 88.2%, respectively. The combination of LRG-1 and CA19-9 was analyzed by fixing the cutoff value at that of CA19-9. The combination of LRG-1 and CA19-9 improved the differential diagnosis between patients with PDAC and HVs, with an increase in AUC of 0.881 and 75.6% sensitivity and 91.7% specificity.

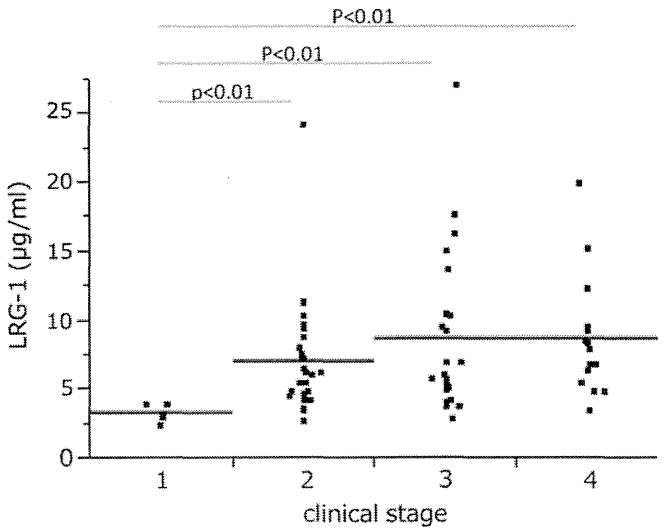

FIGURE 2. Detection of serum LRG-1 in pancreatic cancer patients by enzyme-linked immunosorbent assay. The mean (SD) LRG-1 concentration increased with the progression of clinical stage as follows: stage I, 3.33 (0.66) μg/mL; stage II, 7.07 (4.18) μg/mL; stage III, 8.74 (5.86) μg/mL; and stage IV, 8.72 (4.35) μg/mL. A significant difference was observed between stage I and the other stages, but the differences between stage II and III, III and IV, and II and IV were not significant.

The ability of LRG-1 to make a differential diagnosis between patients with PDAC and patients with CP was also examined. The ROC curve analysis showed that AUC for CA19-9 was 0.913 (Fig. 3B). At a cutoff value of 37 U/mL for CA19-9, the optimal sensitivity and specificity were 73.7% and 100.0%, respectively. Similar analysis for LRG-1 showed AUC of 0.686. At a cutoff value of 4.81 μg/mL for LRG-1, the optimal sensitivity and specificity were 67.7% and 54.3%, respectively. The combination of LRG-1 and CA19-9 enhanced the differentiating power between patients with PDAC and patients with CP, with an increase in AUC to 0.942 with 75.6% sensitivity and 100.0% specificity.

In CA19-9–negative cases, the AUC for LRG-1 was 0.785. At a cutoff value of 4.81 μg/mL for LRG-1, the sensitivity and specificity in differentiating patients with PDAC from HVs were 68.8% and 86.3%, respectively. In regards to differentiating patients with PDAC from patients with CP, the AUC was 0.65, and the sensitivity and specificity were 68.8% and 50.0%, respectively.

LRG-1 Immunohistochemistry

Serum cancer biomarkers can be produced by both cancer cells and the tissues surrounding them. Because LRG-1 is produced in the liver and white blood cells, it is important to identify which cells produce LRG-1 in pancreatic cancer tissue. To address this issue, the pattern of LRG-1 protein expression was assessed by immunohistochemistry using morphological cancer lesions and noncancerous lesions from resection tissue. As shown in Figure 4, pancreatic cancer cells stained positively on the cell sur- F4 face with a plasma membrane staining pattern, but pancreatic duct cells from noncancer cases, including CP and IPMN, did not stain. However, in CP cases, inflammatory cells such as lymphocytes exhibited weak staining. Positive staining was observed in all cases of pancreatic cancer, but a positive signal was scarcely detected in tissue from CP patients or normal surrounding tissue. Serum LRG-1 levels did not correlate with the intensity of immunostaining ($P = 0.327$).

DISCUSSION

We demonstrated that preoperative serum LRG-1 levels are elevated in patients with PDAC compared with HVs and patients with CP. The LRG-1 level is associated with disease progression and

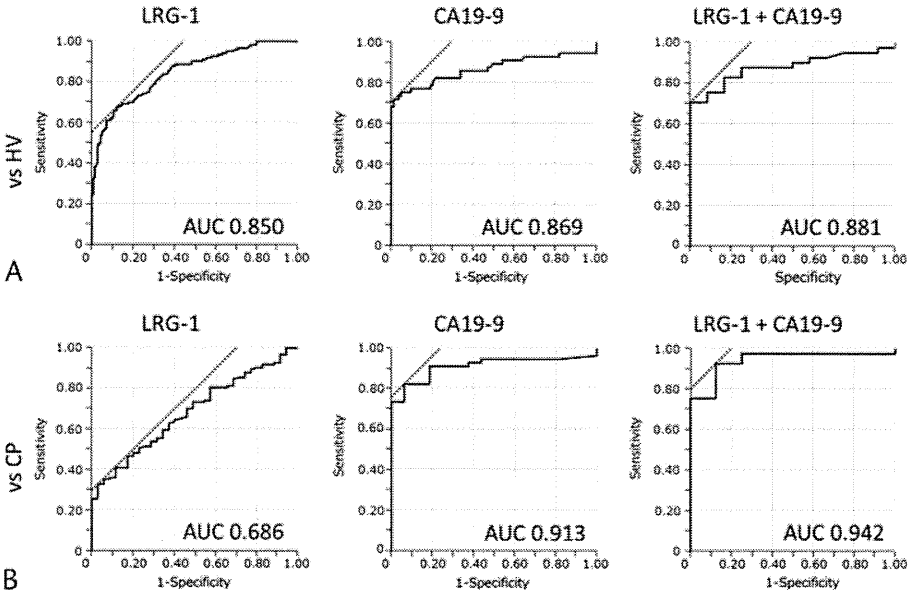

FIGURE 3. Receiver operating characteristic curve analysis for PDAC patients versus HVs (A) and PDAC patients versus CP patients (B). A, Power of LRG-1, CA19-9, and the combination of LRG-1 and CA19-9 in differentiating PDAC patients from HVs. The AUC was 0.850 for LRG-1 alone, 0.869 for CA19-9 alone, and 0.881 for LRG-1 and CA19-9 together. B, Power of LRG-1, CA19-9, and the combination of LRG-1 and CA19-9 in differentiating PDAC patients from CP patients. The AUC was 0.686 for LRG-1 alone, 0.913 for CA19-9 alone, and 0.942 for LRG-1 and CA19-9 together.

lymph node metastasis. Although previous studies have suggested that LRG-1 is induced by both tumor cells and acute/chronic inflammation, serum LRG-1 levels were not as high in the CP patients in our study as previously reported, dues in part to the mild/moderate levels of CP we investigated. Thus, the diagnosis of CP with mild inflammation may be difficult. In contrast, immunohistochemical staining clearly revealed that pancreatic cancer cells, but not noncancer lesions from CP and IPMN cases, were positive for LRG-1. This result suggests that high levels of LRG-1 in pancreatic cancer may be derived from cancer cells or a change in the microenvironment, such as local inflammation associated with cancer progression. However, serum LRG-1 levels did not correlate with staining intensity in tissues, suggesting that serum LRG-1 levels may be dependent on the cleavage of LRG-1 on the cell surface. Andersen et al[9] reported an association between LRG-1 and ovarian cancer. The mean serum LRG-1 concentration was higher in ovarian cancer patients than in healthy women, and highest among stage III/IV patients. Ovarian cancer cells secrete LRG-1, which may contribute directly to the elevated levels of LRG-1 observed in the serum of ovarian cancer patients. Interestingly, the time course is quite different for plasma LRG-1 and CA125. Suboptimal debulking surgery results in a substantial decrease in CA125, whereas LRG-1 levels remain elevated. Thus serum LRG-1 levels seem to be more directly related to tumor burden than CA125.

Initially, LRG-1 was classified as a marker of acute phase inflammatory responses. Serada et al[15] showed that serum LRG-1 concentrations correlate better with disease activity in ulcerative colitis than C-reactive protein. Kawakami et al[19] reported that LRG-1 levels increase after radiofrequency ablation for hepatocellular carcinoma, suggesting a possible role in the acute stress reaction. We confirmed an association between LRG-1 and C-reactive protein in patients with pancreatic cancer ($R^2 = 0.774$, $P < 0.001$). These dual functions of LRG-1 as a tumor marker and acute phase protein prompted us to use it as a marker of tumor recurrence after an acute phase.

We conducted this study to confirm that LRG-1 can be used as a diagnostic marker for PDAC. We found that LRG-1 can distinguish between patients with PDAC and HVs or patients with CP, but we were not able to demonstrate its effectiveness as an early diagnostic marker. However, we confirmed that serum LRG-1 levels are associated with disease progression and lymph node metastasis, and that pancreatic cancer cells express LRG-1 on the cell surface. An analysis of LRG-1 glycosylation may be a promising approach to distinguish cancer-associated LRG-1 from inflammation-associated LRG-1. In the future, if glycan changes in LRG-1 can be used to identify the pancreatic cancer-specific LRG-1, which is different from the LRG-1 protein made by normal cells such as hepatocytes, it may be a more specific biomarker in PDAC.

Leucine-rich α2-glycoprotein-1 was purified more than 30 years ago. The protein contains 8 typical 24-residue leucine-rich repeats with the consensus sequence.[20] However, the physiological function of LRG-1 is still largely unknown. Shirai et al[21] showed that autologous cytochrome *c* (cyt *c*) is an endogenous ligand of LRG-1 and functions in the detoxification of neurotoxins from snake venom. The expression of LRG-1 is up-regulated during neutrophilic granulocyte differentiation in response to G-CSF, suggesting that LRG-1 is involved in granulopoiesis. Leucine-rich α2-glycoprotein-1 functions as 1 of the pattern recognition receptors of polymorphonuclear neutrophils and modulates neutrophil function through innate immunity. Serum LRG-1 concentrations correlate well with disease activity in ulcerative colitis. Recent reports have also demonstrated the diagnostic value of LRG-1 in the urine of children with acute appendicitis. These results support the role of LRG-1 in inflammatory responses. Leucine-rich α2-glycoprotein-1 and Apaf-1 have some amino acid sequence homology, and LRG-1 binding to cyt *c* is similar to that of Apaf-1.[22] However, in contrast to Apaf-1, LRG-1 may clear potentially dangerous cyt *c*. This report suggests a role of LRG-1 in preventing lymphocyte death. When bound to extracellular cyt *c* released from apoptotic cells, serum LRG-1 acts as a survival factor for lymphocytes, and possibly other cells. Moreover, aberrant neovascularization contributes to diseases, such as cancer, and is the consequence of inappropriate angiogenic signaling. The epithelial growth factor receptor and vascular endothelial growth factor are related to angiogenesis, and targeted agents that are capable of